Transportation Research Part C 156 (2023) 104335

Contents lists available at ScienceDirect

Transportation Research Part C

journal homepage: www.elsevier.com/locate/trc

What do we head for while exiting a room? a novel parametric distance map for pedestrian dynamic simulations☆

Fabio Parisi [a], Claudio Feliciani [b], Ruggiero Lovreglio [c,*]

[a] Polytechnic University of Bari, Italy
[b] The University of Tokyo, Japan
[c] Massey University, New Zealand

ARTICLE INFO

Keywords:
Pedestrian Dynamics
Floor Field
Distance Map
Navigation

ABSTRACT

Identifying effective strategies describing crowd dynamics is crucial to enhance simulations of pedestrians for crowded event planning and management. Various modelling solutions have been proposed to describe how people try to exit from a built environment in normal and emergency. Several of these solutions rely on the use of distance maps or floor fields to account for the positions of existing goals and the location of obstacles to avoid. To date, distance maps are assumed to be static (they do not vary over time) and that pedestrians aim at the actual central coordinate of a door.

In this work, we challenge the static goal assumption by proposing a novel parametric distance map which is variable depending on the polar coordinates defining the position of a pedestrian having the centre of an exit as the origin (i.e., the distance of the pedestrian and an angle between its direction and the perpendicular to the exit). In this work, we investigate what pedestrians head for while trying to reach an exit. Different parametric solutions are proposed and calibrated using likelihood-based optimisation methods with over 9000 trajectories of individual pedestrians who navigated through an indoor university atrium building to reach several exits. The results highlight good performance for this modelling approach: pedestrians head for targets in front of an exit when they are away from it, and their targets shift behind the exit as they get closer to it, (i.e., distance impact) while their angle does not have impact on this process. The proposed dynamic goal-based distance map can be applied for future pedestrian simulations for crowded event planning and management.

1. Introduction

Given the increment in the demand for mass events, pedestrians are more likely to gather in buildings and transportation terminals with limited spatial resources (Johansson et al., 2012), sometimes resulting in accidents due to a lack of planning and preparedness or because available technologies are not sufficiently utilised (Haghani & Lovreglio, 2022). In fact, since 2008, over 50% of the world's population has been living in cities, and this percentage is predicted to increase dramatically by the end of this century (Johansson

☆ This article belongs to the Virtual Special Issue on "special issue full title".

* Corresponding author at: School of Built Environment, Massey University, East Precinct Albany Expressway, SH17, Albany, Auckland 0632, New Zealand.
E-mail address: r.lovreglio@massey.ac.nz (R. Lovreglio).

https://doi.org/10.1016/j.trc.2023.104335
Received 18 April 2023; Received in revised form 1 September 2023; Accepted 6 September 2023
Available online 21 September 2023

et al., 2012) (UN Population Division, 2007) (Feliciani & Nishinari, 2018). Pedestrian crowds will become a more relevant feature of large cities by occurring not only during mass gatherings but also at routine events such as commuting to work. As such, it is critical to have a reliable understanding of the behavioural rules that describes how pedestrian move and navigate in the built environment expanding the existing state of the art (Hänseler et al., 2017) (Haghani & Sarvi, 2018) (Haghani, 2020) (Haghani, 2020) (Duives et al., 2013) (Feng et al., 2021).

Pedestrian motion is the result of several behavioural rules which can be subdivided into three levels, typically divided into the strategic, tactical, and operational levels (Hoogendoorn & Bovy, 2004). These levels define how people take decisions (strategic), plan their route (tactical) and actually move (operational) inside any given environment. This decision-making subdivision is intended to provide a theoretical framework for developing of simulation models and planning pedestrian infrastructure and transportation facilities. Usually, it is employed at large scales (city, neighbourhood, building, etc.) where trip origin–destination plays an important role, but the same concept could be used also on a smaller scale to describe the way people move inside a room, for instance. The latter approach has generally received less attention from researchers since the shortest path is usually assumed to be enough to explain pedestrian behaviour at the microscopic level.

To date, multiple modelling solutions have been proposed to describe how pedestrians navigate in normal conditions and to simulate the evacuations of the built environment during an emergency (Haghani & Sarvi, 2018) (Kuligowski et al., 2010) (Kuligowski, 2016) (Zanlungo et al., 2023). When focusing on microscopic pedestrian modelling solutions, these can be subdivided into continuous models (see the example of the Social Force Model (Moussaïd et al., 2011)) and discrete models (see the example of the Cellular Automata Model (Burstedde et al., 2001) (Kirchner & Schadschneider, 2002)) depending on how the space is discretised (Moustaid & Flötteröd, 2021) (Guo & Huang, 2012). These solutions have been implemented today in multiple pedestrian and evacuation dynamics software packages (Kuligowski, 2016) (Lovreglio et al., 2019).

Several existing pedestrian and evacuation modelling solutions rely on the use of distance maps as the fundamental modelling layer. Fundamental maps are also referred to as floor fields or potential maps, while their normalised gradients are generally named desired direction fields[1] (Burstedde et al., 2001) (Karmakharm et al., 2010) (Thompson & Marchant, 1995) (Kretz et al., 2011) (Lovreglio et al., 2018). Distance maps are used in the pedestrian dynamics domain to provide each simulated pedestrian with desired directions to move towards and avoid, accounting for the positions of existing goals and the location of obstacles (Lovreglio et al., 2018). As such, distance maps are a fundamental modelling layer in many pedestrian dynamic solutions to identify at each simulated time step where a pedestrian would be aiming at in case there are no interactions with other pedestrians (Guo & Huang, 2012). It is worth highlighting that the distance map layer is conceptually different from the classical routing problem investigated in exit choice or route choice studies, which represent another model layer (Chraibi et al., 2013). Distance maps are fundamental when using several popular continuous pedestrian evacuation models, such as Simulex (Thompson & Marchant, 1995) and Pathfinder (Thunderhead Engineering, 2022). Further, distance maps are helpful when implementing the well-established Social Force Model (Kretz et al., 2011) (Korhonen, 2017) (Anvari et al., 2015) to define the desired direction of motion for a pedestrian if there are no other pedestrians to interact with (Helbing et al., 2000). Finally, distance maps represent a fundamental modelling layer for a class of discrete pedestrian models, namely, floor field Cellular Automata models (Li et al., 2019) (Lu et al., 2017) (Hsu & Chu, 2014) (Fu et al., 2018).

Several approaches have been used so far to define distance maps for pedestrian and evacuation models, which can be subdivided into theoretical and data-driven solutions. The most common theoretical metric used to define distance maps is Euclidean distance which is ideal when there are no obstacles in a room (Guo & Huang, 2012). However, other theoretical metrics have been proposed and tested, such as the Dijkstra distance (Lu et al., 2017) (Hsu & Chu, 2014) (Fu et al., 2018) (Nishinari et al., 2004) and Manhattan distance (Varas et al., 2007) (Alizadeh, 2011) or combinations of them (Huang et al., 2022) for spaces having obstacles in them. In some other cases, distance maps are built using a fluid dynamic simulator on a two-dimensional grid (Korhonen, 2017) or by using algorithms based on the distribution of space potential (Guo & Huang, 2012). Other theoretical attempts for 90 and 180 bends were proposed by (Steffen & Seyfried, 2009), while (Chraibi et al., 2013) tested different assumptions on which goals pedestrian aim at while approaching an exit using simulations.

More recently, novel distance maps have been proposed using data from pedestrian experiments and field observations. For instance, data from immersive virtual reality experiments were used in (Lovreglio et al., 2015) to estimate distance maps for pedestrians evacuating a road tunnel. In (Dias & Lovreglio, 2018), data from a pedestrian experiment were used to predict the distance maps of pedestrians walking around 90° bends. Finally, data from field observation were used by (Corbetta et al., 2015) and (Lovreglio et al., 2018) to predict pedestrian navigation maps in a U-shaped landing corridor and an indoor university atrium, respectively. In all these previous studies, distance maps are assumed to be static; namely, they do not vary over time as the pedestrian objectives do not vary (i.e., the *static assumption*). For instance, these existing maps rely on the assumption that pedestrians aim at the actual central coordinate of an exit during the full navigation process leading them out of that existence, and the pedestrians' goal is static over time. To the best of our knowledge, this assumption has not been questioned and challenged in previous works.

In this work, we challenge the static goal assumption by proposing a novel parametric distance map which assumes that pedestrian goals change over time while approaching an exit and going through such an exit. To achieve this aim, we investigate what pedestrians aim at while trying to reach an exit and if/how their goals vary over time. In this work, we use over 9000 trajectories of individual

[1] From a mathematical perspective, a distance map is a function defined as M: $R^2 \rightarrow R$. As such it assigns to each pair (x,y) in the physical walking space a scalar value which represents the "distance" of that point to the final objective. On the other hand, the gradient of M is a vector field (∇M: $R^2 \rightarrow R^3$) that can be used to identify the desired direction field (F) by taking the projection of the gradient on the x-y plane and normalizing it. This vector field associates to each pair (x,y) in the physical walking space a unit vector representing the desired direction for a pedestrian (F: $R^2 \rightarrow R^2$).

pedestrians (who navigated through an indoor university atrium building to reach several exits) to test different parametric distance maps.[2] These novel dynamic goal-based distance maps are estimated using likelihood-based optimisation methods, which allow identifying which map provides the best description of the data. Finally, the proposed new distance map is compared with traditional maps through a couple of modelling assessment procedures.

2. Material and methods

In this work, we propose a new parametric distance map to describe the movement of a pedestrian to reach an exit. The conceptual idea underpinning this new distance map is described in Section 2.1. The model specification, the calibration algorithms, and model comparison tests adopted in this work are reported in Section 2.2. Finally, the dataset used to calibrate and test the proposed solution is described in Section 2.3.

2.1. Conceptual model

When modelling pedestrian movement, the behavioural algorithms describing the movement of individuals are subdivided into three levels, which include the strategic level, tactical level, and operational level (Hoogendoorn & Bovy, 2004). At the operational level, the main modelling objective is to describe how a pedestrian tries to reach a goal (e.g., an exit) while interacting with others. Distance maps are traditionally used to define how a simulated pedestrian will reach its goal. One of the most common assumptions adopted in the literature is to assume that the pedestrian goal is the central location of an exit (Burstedde et al., 2001) (Kirchner & Schadschneider, 2002) (Chraibi et al., 2013) (Helbing et al., 2000). This assumption has been previously tested in previous calibration studies (Lovreglio et al., 2018) (Lovreglio et al., 2015). However, different solutions have been proposed to deform the traditional Euclidian distance maps to generate solutions closer to the observed pedestrian data in the proximities of the exit. Deforming the Euclidean matrix allowed the generation of curved trajectories, but such a solution does not explain the real behavioural rule describing how pedestrians behave while reaching an exit.

In this work, we tested a new behavioural rule based on the assumption that pedestrians change their goal over time while approaching an exit and going through such an exit. The proposed conceptual model assumes that pedestrians aim at goals in front of the exit while relatively distant from an exit and that the desired goals get closer to the central location of the exit. When pedestrians are relatively close to the exit, their goals go behind the exit in the new space they are about to access.

The proposed modelling approach is mostly inspired by everyday experience when transiting through doors or gates,[3] but it is possible to identify a few cognitive factors explaining this peculiar behaviour. Humans are typically known to have functional asymmetry, which is manifested in preferential writing and turning directions (Lenoir et al., 2006). However, humans have been also shown to navigate using specific references, for example the sun in an outdoor environment (Souman et al., 2009) and the walls when navigating indoor (Sussman & Hollander, 2021). (Sussman & Hollander, 2021) describes how people tend to avoid “empty spaces” and seek the protection of walls, leading to the “wall-hugging” trait. However, while walls have a reassuring function, edges are a source of uncertainty as it cannot be predicted what would lie behind. To summarise, it is therefore possible that the tendency of passing straight through gates is a combination of the following factors: 1) enable to visually inspect behind the edge as one approaches toward an exit and 2) use structural elements as a reference to orientate one’s moving direction.

Fig. 1 provides a visualisation of the conceptual modelling solution proposed in this work showing the moving goal hypothesis driving the pedestrian movement. This figure shows a pedestrian moving towards an exit at different four-time steps (i.e., t_0 - t_4). While the pedestrian gets close to the exit, the position of the desired goal moves from a location in front of the exit to a location behind the exit. Further, we make the following assumptions.

(a) The desired goals are located on the perpendicular axis passing from the central location of an exit (see the dashed line in Fig. 1).
(b) The location of the desired goals is a function of both the distance of a pedestrian from the central location of an exit (d) and the θ angle shown in Fig. 1. In other words, the location of the desired goals is a function of the polar coordinate defining the location of a pedestrian using the exit location and orientation as a reference point.

Different modelling formulations are tested in this work to specify this function, as shown in Section 2.2.

2.2. Model specification

Based on the conceptual model described in Section 2.1, we have specified different model equations for the distance maps (D), which can integrate the assumptions that pedestrians’ goals change as they approach an exit. To achieve this goal, we define the following generalised Equation (1), expanding on the modified Euclidean metric proposed by (Lovreglio et al., 2018).

[2] As such, we aim to reproduce a non-emergency situation where people leave a room without an overwhelming time pressure in doing so. In this regard, we want to stress that crowd simulation in the case of emergency has already reached a considerable degree of accuracy. Nowadays, crowd simulation software is also often used to model pedestrian behaviour in daily situations, thus highlighting the need to accurately estimate space utilization and improve attractiveness and efficiency of pedestrian facilities.

[3] This observation is further backed by the experimental data collected which will be presented later.

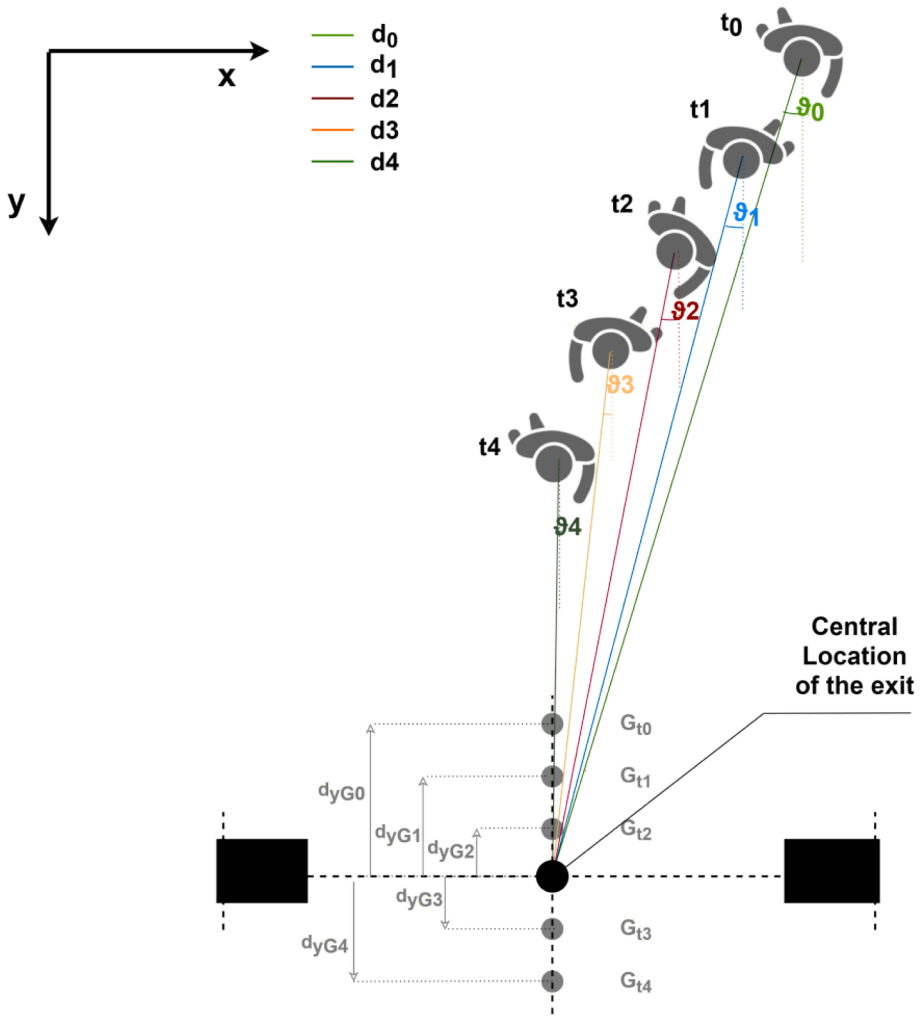

Fig. 1. Visualisation of the moving desired goal over the four-time steps t_0-t_4.

$$M = \sqrt{(x - X)^2 + \alpha\left(y - \left(Y + d_{yG}\right)\right)^2} \tag{1}$$

where α is the global distortion parameter; x and y are the coordinates defining the position of the pedestrian, as specified by the reference system in Fig. 1; X and Y are the coordinates defining the position of the location of the centre of an exit. Finally, d_{yG} is a parameter (measured in meters) representing the variation of the pedestrian goal while approaching the exit, and it is the core part of the investigation in this study. A visualisation of d_{yG} and its variation is illustrated in the conceptual model proposed in Fig. 1: negative values imply that the goal aimed is closer to the pedestrian (and inside the room), while positive ones imply the opposite.

In this work, we tested and compared different model specifications for the d_{yG} term. A summary of the model specifications tested in this work is provided in Table 1. The equations in Table 1 show that we tested several linear and non-linear models defining the relationship between d_{yG} term, the distance d of the pedestrian from the exit and the θ angle as defined in Fig. 1. We started investigating separately the linear dependency of d_{yG} on d (models M1-U and M1-C) and θ (models M2-U and M2-C) to preliminary detect eventual prevalent informative content among them. Due to the informative prevalence of d over θ (this trend is shown in the results section in Table 4), we progressively added complexity to models M1-U and M1-C and used them as baselines, further specifying:

i) non-linear dependency on d (models M4-U and M4-C);
ii) linear dependency on θ (models M3-U and M3-C), and
iii) their combination (models M5-U, M5-C, M6-U, M6-C).

Fig. 2 shows the structure of the models specified in this work by classifying them into models without global distortion parameters (i.a., the α parameter is constrained to one) and models with global distortion parameters (i.a., the α parameter is unconstrained).

Table 1
Variation of the pedestrian's goal position in the different Distance Maps investigated.

Model ID	Formulation description	d_{yG}	α
M0-U	Euclidean metric with global distortion parameter	0	unconstrained
M0-C	Euclidean metric without global distortion parameter	0	constrained to 1
M1-U	Linear in d, with global distortion parameter	$k_1 + k_2 \cdot d$	unconstrained
M1-C	Linear in d, without global distortion parameter	$k_1 + k_2 \cdot d$	constrained to 1
M2-U	Linear in θ, without d dependency, with global distortion parameter	$k_1 + k_5 \cdot \lvert\theta\rvert$	unconstrained
M2-C	Linear in θ, without d dependency, without global distortion parameter	$k_1 + k_5 \cdot \lvert\theta\rvert$	constrained to 1
M3-U	Linear in d, with θ dependency, with global distortion parameter	$k_1 + k_2 \cdot d + k_5 \cdot \lvert\theta\rvert$	unconstrained
M3-C	Linear in d, with θ dependency, without global distortion parameter	$k_1 + k_2 \cdot d + k_5 \cdot \lvert\theta\rvert$	constrained to 1
M4-U	Non-linear polynomial in d, with global distortion parameter	$k_1 + k_2 \cdot d + k_3 \cdot d^{k_4}$	unconstrained
M4-C	Non-linear polynomial in d, without global distortion parameter	$k_1 + k_2 \cdot d + k_3 \cdot d^{k_4}$	constrained to 1
M5-U	Non-linear polynomial in d, with θ dependency, with global distortion parameter	$k_1 + k_2 \cdot d + k_3 \cdot d^{k_4} + k_5 \cdot \lvert\theta\rvert$	unconstrained
M5-C	Non-linear polynomial in d, with θ dependency, without global distortion parameter	$k_1 + k_2 \cdot d + k_3 \cdot d^{k_4} + k_5 \cdot \lvert\theta\rvert$	constrained to 1
M6-U	Non-linear polynomial both d and θ, with global distortion parameter	$k_1 + k_2 \cdot d + k_3 \cdot d^{k_4} + k_5 \cdot \lvert\theta\rvert + k_6 \cdot \lvert\theta\rvert^{k_7}$	unconstrained
M6-C	Non-linear polynomial both d and θ, without global distortion parameter	$k_1 + k_2 \cdot d + k_3 \cdot d^{k_4} + k_5 \cdot \lvert\theta\rvert + k_6 \cdot \lvert\theta\rvert^{k_7}$	constrained to 1

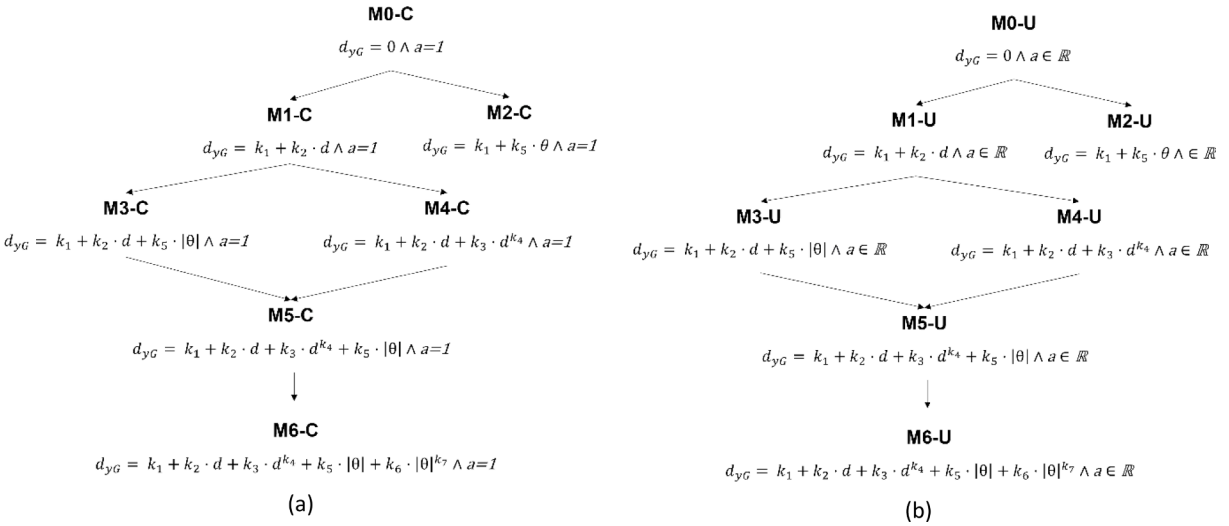

Fig. 2. Structure of the proposed specifications in Table 1 subdivided in (a) models without global distortion parameter, $\alpha = 1$; and (b) models with global distortion parameter,.$\alpha \in R$

2.3. Model calibration

To calibrate different distance maps and compare them, we use the calibration procedure based on floor field cellular automata models (Burstedde et al., 2001) (Kirchner & Schadschneider, 2002), which use a traditional multinomial logit formulation to predict how pedestrians move in a simulated walkable space proposed in (Lovreglio et al., 2015). As such, this method relay on the optimisation of a log-likelihood function to identify the parameters which provide a better fitting with the data. Likelihood-based optimisation methods for multinomial logit models are already established in the transportation field, and many tools are available for model estimation in R (Hess & Palma, 2019) (Molloy et al., 2021), Python (Bierlaire, 2020) or other different languages or executable software (such as MATLAB being used here) (Hensher et al., 2005), which often allow for modelling specifications based on linear formulations. We coded the log-likelihood functions for the specified model in MATLAB, and we adopted a Quasi-Newton method based on gradients to identify the optimal point of the proposed log-likelihood functions. We used the MATLAB function *fminunc* to perform a non-linear unconstrained optimisation employing the Hessian approximation updating inspired by the Broyden–-Fletcher–Goldfarb–Shanno (BFGS) method (Feliciani et al., 2020) (Ioannidis, 2019) (Gwynne & Rosenbaum, 2016) (Purser, 2010).

The log-likelihood equation used in this work is a modification of the one originally proposed in (Lovreglio et al., 2015) based on the assumptions of well-established *floor field cellular automata models* (Burstedde et al., 2001) (Kirchner & Schadschneider, 2002). This pedestrian modelling framework relies on the following assumptions.

(a) The space walkable by pedestrians is subdivided into cells which can either be empty or occupied by one pedestrian. Different shapes of cells could be used, such as triangular, square, and hexagonal (Dias & Lovreglio, 2018) (Torrens, 2009). The main aim

of this work is to compare different models, and thus cell geometry plays a marginal role (as long as the same is used for all models). Thus we decided to focus on square meshes, which are the most popular when using this type of modelling, given its simple implementation (Li et al., 2019).

(b) The Moore neighbourhood assumption allows pedestrians to move locally to any of the eight cells surrounding the cells they are occupying (L_{ij}) where *(I,j)* is the location of the cell, as illustrated in Fig. 3.

(c) Pedestrians can change their location after a fixed time step interval.

(d) A q pedestrian assign to each possible location a utility which is a function of the distance map (D_{ij}^{q}) (also known as a static distance map) and a dynamic distance map. The dynamic distance map considers the location of other pedestrians and is not included in the following part of the formulation, given the nature of this study.[4] As such, the utility function of the q pedestrian can be specified, as shown in Equation (2).

$$U_{r,s}^{q} = k_s M_{r,s}^{q} + \varepsilon \tag{2}$$

where $r \in \{i-1, i, i+1\}, s \in \{j-1, j, j+1\}$ and ε is the error term associated with those utilities and $M_{r,s}^{q}$ have the formulation shown in Equation (1) and Table 1. Finally, k_s is the parameter defining the weight of the distance map on the local moving process.

(e) The ε error term follows generalised extreme value distribution Type-I. As such, a multinomial logit formulation can be used to predict the probability that the q pedestrian will move to the L_{rs} cell (see Equation (3).

$$p_{r,s}^{q} = \frac{e^{(k_s M_{r,s}^{q})}}{\sum_{(r,s)} e^{(k_s M_{r,s}^{q})}} \tag{3}$$

Under these assumptions, it is possible to define a likelihood function to estimate the unknown parameters using observed choices made by pedestrians by sampling them from their trajectories. This process was originally introduced in (Lovreglio et al., 2015), and it is summarised in the following paragraphs.

Assuming that $\boldsymbol{T^q} = \{\boldsymbol{L_1^q}, \cdots, \boldsymbol{L_t^q}, \cdots, \boldsymbol{L_n^q}\}$ is the n-vector, including all the observed cells occupied by the q pedestrian for each consecutive time step ($t = 1,\ldots,n$). The probability of the q pedestrian passing from $\boldsymbol{L_t^q}$ to $\boldsymbol{L_{t+1}^q}$ can be defined by Equation (4):

$$P\left(\boldsymbol{L_t^q} \rightarrow \boldsymbol{L_{t+1}^q}\right) = p^{q}\left(\boldsymbol{L_t^q}, \boldsymbol{L_{t+1}^q} \middle| k_s, \boldsymbol{\beta}\right) \tag{4}$$

where k_s and $\boldsymbol{\beta}$ (i.e., the vector of parameters defining the distance map shown in Table 1) are the unknown parameters to estimate. The probability of pedestrian q having the $\boldsymbol{T^q}$ trajectory can be shown in Equation (5).

$$P(\boldsymbol{T^q}) = \prod_{t=1}^{n-1} P\left(\boldsymbol{L_t^q} \rightarrow \boldsymbol{L_{t+1}^q}\right) \tag{5}$$

The likelihood function of the sample of Q observed pedestrians can be written as shown in Equation (6).

$$L(\boldsymbol{\beta}, k_s) = \prod_{q=1}^{Q} P(\boldsymbol{T^q}) \tag{6}$$

The variables of this function are the parameters that need to be calibrated (i.e.,$\boldsymbol{\beta}, k_s$). Thus, these parameters can be estimated by maximising $L(\boldsymbol{\beta}, k_s)$**.** For convergence reasons, it is more common to use the log-likelihood function rather than the likelihood function itself as shown in Equation (7) (Hensher et al., 2005) (Greene, 2011).

$$LogL(\boldsymbol{\beta}, k_s) = \sum_{q=1}^{Q} \boldsymbol{log}(P(\boldsymbol{T^q})) \tag{7}$$

2.4. Model comparisons

Different model specifications are proposed in this work, as shown in Table 1. Thus, it is fundamental to use criteria to compare the proposed model estimation. Different criteria have been proposed in the literature and adopted to compare nested and non-nested models in the transportation domain (Shen, 2009) (Cerwick et al., 2014). In line with the existing literature, the comparison is carried out in this work by using the following criteria and tests listed in Table 2, which includes the adjusted McFadden R-Squared (AMFR^2), the Akaike Information Criterion (AIC) and Bayesian Information Criterion (BIC).

[4] The dynamic distance map plays an important role in the case of emergent structures, for example lanes in a corridor. In the absence of group dynamics and if people mostly behave at an individual level simply avoiding physical interactions with others, ignoring the dynamic distance map will not affect the outcome.

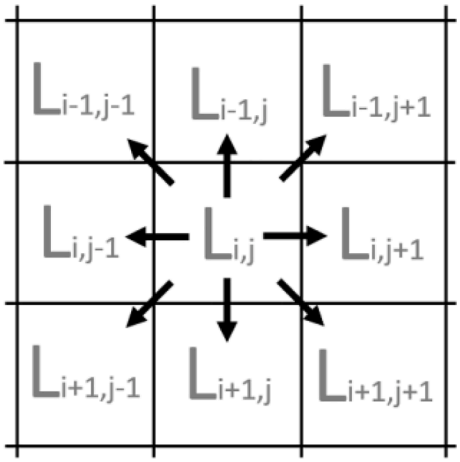

Fig. 3. The Moore neighbourhood assumption for local pedestrian movement.

Table 2
Comparison criteria.

Name	Equation
Adjusted McFadden R-Squared ($AMFR^2$)	$AMFR^2 = 1 - \frac{LogL(M) - K}{LogL(M_0)}$ where K is the number of parameters, M is the model the metric applies to and M_0 is model with a constant only
Akaike Information Criterion (AIC)	$AIC = 2K + 2LogL(M)$ where K is the number of parameters and M is the model the metric applies to
Bayesian information criterion (BIC)	$BIC = -2LogL(M) + \log(N)*K$ where K is the number of parameters and M is the model the metric applies to and N is the number of observations

2.5. Trajectory dataset

In this work, we use the open pedestrian trajectory dataset collected in the Informatics Forum building of the University of Edinburgh (UK) to compare the different model specifications proposed in Section 2.2. The original dataset published by (Majecka, 2009) contains 299,082 pedestrian trajectories of people walking Informatics Forum building in normal situations. The trajectories were collected by the authors using a 640 × 480 resolution camera located about 23 m above the floor with a frame rate of 9 fps for a period of 117 days (see Fig. 4). The original data is available in 117 text files, including the coordinates of all the individuals walking in the atrium. This data was lately imported in a single MATLAB dataset by Lovreglio et al. (Lovreglio et al., 2018) (Lovreglio et al., 2017), which is the dataset used in this work. This dataset converted the measure in pixels provided by Majecka et al. (Majecka, 2009) in a new reference system in meters using the real distance information displayed in Fig. 4.

The nature of this study lies in the investigation of how pedestrians move to reach an exit without interacting with other pedestrians. As such, to calibrate the distance maps specified in Section 2.2 we used only the trajectories of pedestrians walking individually in the atrium while trying to reach an exit. Since the top view of the camera does not allow a clear identification of the location of the exits, we only use the trajectories of the pedestrian exiting using the doors on the bottom in Fig. 4, being clearly visible targets in the recorded scenes. Further, we filtered through all the trajectories of pedestrians who were only aiming at exiting doors instead of taking multiple actions and reaching different goals in the atrium, which were not doors. This filtering was carried out to verify that pedestrians were reducing his/her distance from the goal door at each time step. The final dataset used in this study consists of 9,239 trajectories. These trajectories are illustrated in Fig. 5 for each exit.

To generate data suitable with the discrete choice calibration solution described in Section 2.2, the decisions made by the pedestrian are detected using each trajectory by subdividing the atrium into square cells of 0.1 × 0.1 m^2. In fact, as shown in the analysis carried out in (Lovreglio et al., 2018), the probability of a pedestrian moving to a new adjacent cell at each time step is above 95%. This space discretisation is fundamental to creating the dataset, including all the choices made by each pedestrian at each time interval and associating them to the location of the pedestrian when the choices were made. Using this approach, it was possible to sample 488,655 choices out of the 9,239 trajectories used in this work and link to them the pedestrians' locations.

3. Results

The results of the estimated parameters for the model specification in Table 3, as well as the fitting performance of the models, are proposed in Section 3.1. A sensitivity analysis of the best-performing models is described in Section 3.2. Finally, the property of the selected distance map is visualised and described in Section 3.3.

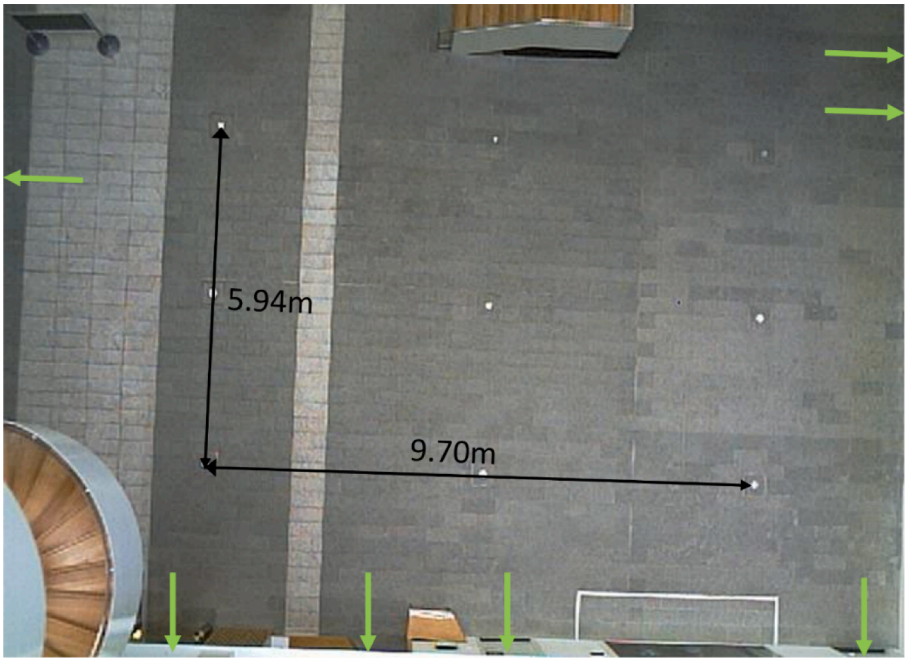

Fig. 4. Top view of the empty atrium layout from the camera. The green arrows represent the locations of the exits. Figure modified from Majecka et al. (Majecka, 2009). (For interpretation of the references to colour in this figure legend, the reader is referred to the web version of this article.)

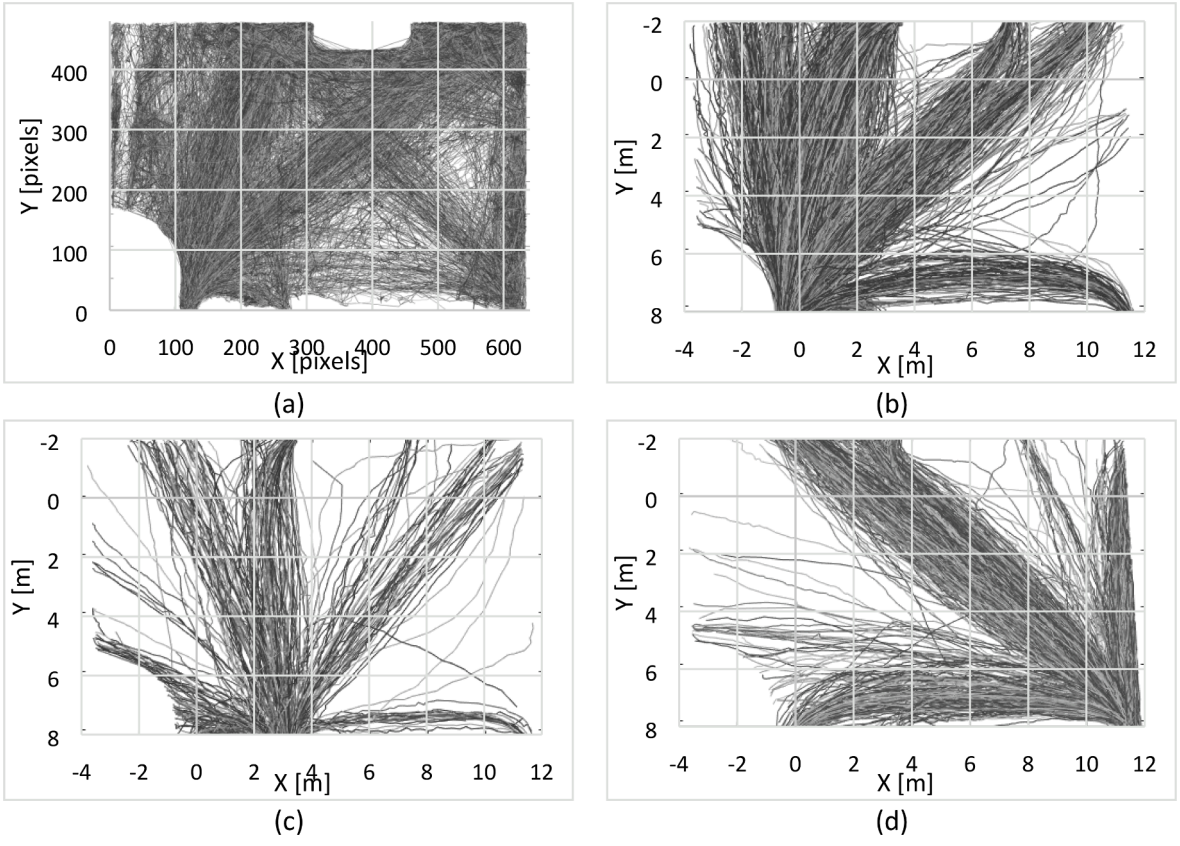

Fig. 5. Visualisation of (a) the unfiltered trajectories in the original pixel coordinates; (b) the filtered trajectories of the pedestrian using the left exit; (c) the filtered trajectories of the pedestrian using the central exit; (d) the filtered trajectories.

Table 3
Estimated parameters.

Model	Ks	a	k1	k2	k3	k4	k5	k6	k7
M0	0	0	0	0	0	0	0	0	0
M0-U	−36.002	0.768	0	0	0	0	0	0	0
M0-C	–33.046	1	0	0	0	0	0	0	0
M1-U	−42.549	1.22	0.146	−0.306	0	0	0	0	0
M1-C	−42.545	1	0.240	−0.263	0	0	0	0	0
M2-U	−37.744	6.584	2.057	0	0	0	0.612	0	0
M2-C	–33.643	1	0.597	0	0	0	−0.328	0	0
M3-U	−42.582	1.191	0.143	−0.298	0	0	−1.44e-02	0	0
M3-C	−42.333	1	0.176	−0.253	0	0	−2.68e-02	0	0
M4-U	−41.509	1.246	–23.806	−0.256	23.784	−2.6e-03	0	0	0
M4-C	−41.039	1	–23.795	−0.193	2.380	−2.7e-03	0	0	0
M5-U	−40.620	1.257	0.224	−1.84e-02	−0.526	−0.672	−5.2e-05	0	0
M5-C	−40.316	1	0.260	4.48e-02	−0.550	0.662	−3.8e-04	0	0
M6-U	−40.983	1.262	0.234	−2.45e-02	−0.528	0.669	0.119	−0.1203	0.997
M6-C	−40.567	1	0.272	4.05e-02	−0.552	0.659	0.118	−0.1195	0.997

3.1. Estimated models

We report here the parameters estimated for all the models with the optimisation procedure in Table 3 and their fitting performance in Table 4.

The results in Tables 3-4 highlight that adding complexity results in a better fitting. In fact, M6-U has the highest log-likelihood value and the best overall fitting in terms of higher $AMFR^2$ and lower AIC and BIC. The models implementing only the dependency on θ perform the worst, and this evidence leads us to not consider them as a baseline to develop more complex models based on their formulation (as shown in Fig. 2, where there is no model derived from M2-C and M2-U). Among the models of intermediate complexity, M4-U is not dependent on θ and shows good fitting performances.

Despite their fitting performance, the models also need to be evaluated based on their physical interpretation to assess how the different parameters affect the results of the distance map. This is done in the following section. In fact, although the fitting performance of the proposed model specification indicates that both d and θ have an impact on pedestrian navigation, this was an expectable result given the dataset size. As such, the sensitivity analysis carried out in Section 3.2 represents a valuable tool for selecting the final model specification for this work.

3.2. Sensitivity analysis

The estimated results proposed in Section 3.1 allowed us to investigate the influence of the variables d and θ on the different distance map formulations. In this analysis, we consider the two models, M4-U and M6-U. The M6-U model was selected for its fitting performance and for accounting for both the impact of d and θ. On the other hand, M4-U, for its fitting performance when θ is not included in the model specification.

First, the analysis focuses on the d_{yG} functions of the two selected model specifications (M4-U and M6-U). The relationship between d_{yG} and d is displayed in Fig. 6, where negative d_{yG} values represent the moving goal inside the walkable space. The two formulations show a similar trend, and both visualise the hypothesis of the moving goal: starting from the actual goal, the pedestrians aim at a goal that is moving beyond the real exit. Before this distance, they aim instead at a goal that is closer to their position, and this evidence is

Table 4
Performance and statistical test of the estimated models.

Model	LL	$AMFR^2$	AIC	BIC
M0	–	–	–	–
M0-U	−482810	0.553	9.606e + 05	9.607e + 05
M0-C	−480320	0.550	9.656e + 05	9.656e + 05
M1-U	−466800	0.565	9.336e + 05	9.337e + 05
M1-C	−467900	0.564	9.359e + 05	9.360e + 05
M2-U	−474882	0.558	9.498e + 05	9.498e + 05
M2-C	−481724	0.551	9.635e + 05	9.635e + 05
M3-U	−466600	0.565	9.333e + 05	9.333e + 05
M3-C	−467500	0.565	9.351e + 05	9.351e + 05
M4-U	−463300	0.569	9.266e + 05	9.267e + 05
M4-C	−464900	0.567	9.299e + 05	9.300e + 05
M5-U	−461100	0.570	9.222e + 05	9.222e + 05
M5-C	−462500	0.569	9.251e + 05	9.251e + 05
M6-U	−460900	0.571	9.217e + 05	9.218e + 05
M6-C	−462300	0.569	9.247e + 05	9.248e + 05

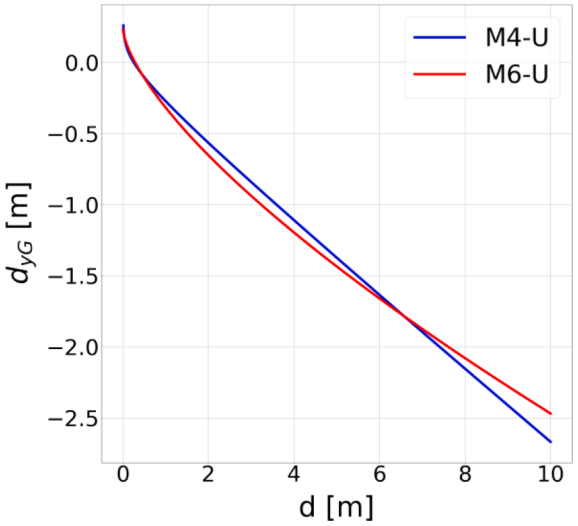

Fig. 6. Comparison of d_{yG} from the models M4-U (in blue) and M6-U (in red). (For interpretation of the references to colour in this figure legend, the reader is referred to the web version of this article.)

highlighted by the negative value of d_{yG}.

Second, we focus on the impact of θ on the distance map running a sensitivity analysis of M6-U. Fig. 7 and Fig. 8 report noticeable features of the model M6-U specifically, highlighting the influence of the parameter θ on its formulation. Fig. 7 represents the d_{yG} curves of the model M6-U with different values of θ, showing its dependency on this variable: it is quite evident that the actual influence of θ is negligible since the curves are overlapped. Fig. 8 depicts the d_{yG} curves of the same model as a function of θ for different values of d. The curves are similarly shaped (since there is no dependency between θ and d), and they appear mainly flat for all the values of θ, implying no dependency of d_{yG} on this variable.

The negligible influence of the variable θ is further highlighted by Fig. 9 and Fig. 10, which represent the dependency of d_{yG} for both the model on both θ and d. Despite being d_{yG} of M6-U dependent on θ, the global shape of the d_{yG} function is quite similar to M4-U, assessing clearly that d is the only variable that has a clear influence on d_{yG} and, thus, the distance map. Based on this evidence, we selected the M4-U model specification in section in Section 3.3 to highlight the properties of the selected distance maps.

3.3. *Distance map properties*

This section focuses on the distance map when selecting M4-U specification for d_{yG}. To highlight the properties of this distance map, Fig. 11 compares it with the baseline Euclidean distance map. This figure shows the projection of the distance maps on the plane x-y,

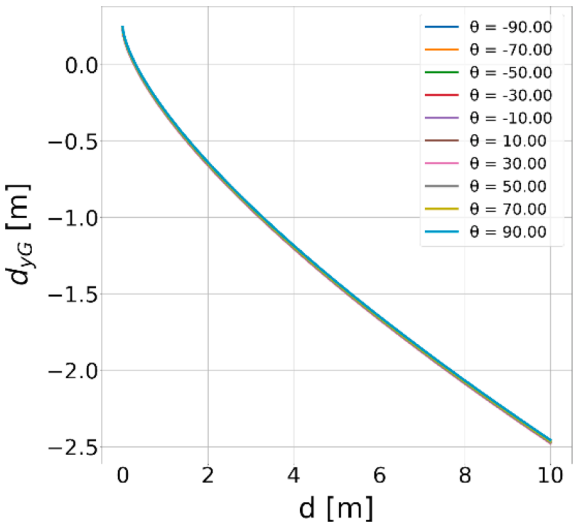

Fig. 7. d_{yG} curves of the model M6-U with values of θ varying in [-90,90]deg.

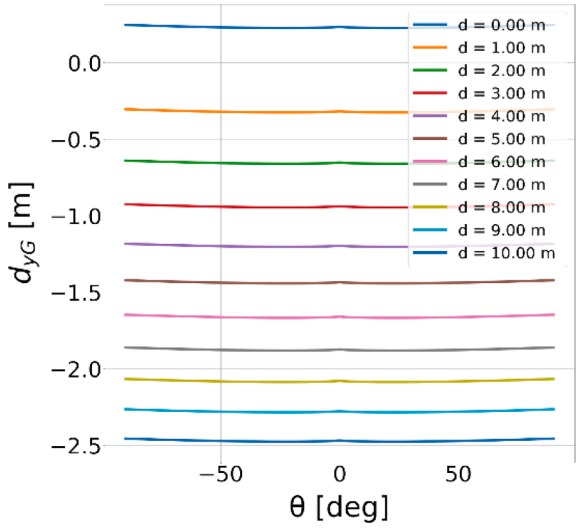

Fig. 8. d_{yG} curves of the model M6-U with values of d varying in [0,10]m.

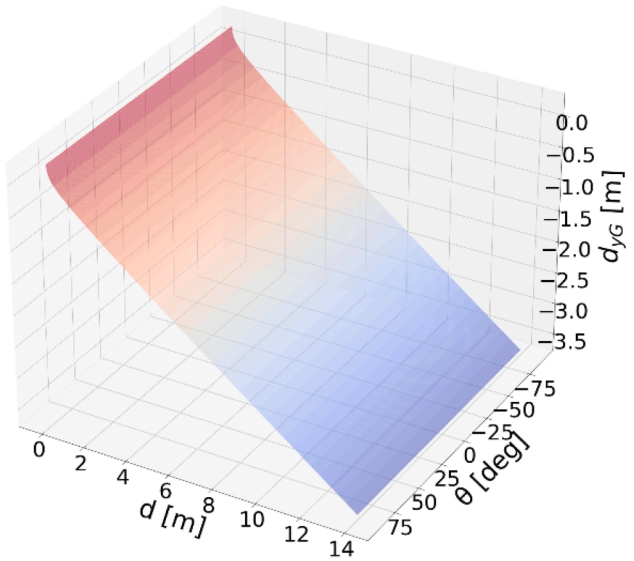

Fig. 9. d_{yG} representation function of d and θ in the model M4-U.

also highlighting the trajectories followed by the pedestrian in the two different cases. M4-U in Fig. 11 features a shape that varies while the distance from the exit increases so that the change in its convexity is evident. This particular characteristic can better represent those trajectories of pedestrians walking between goals and starting points located on the same side of the walkable environment: pedestrians walk away from the exit, step inside the walkable environment and proceed far from the walls with a curved trajectory and then aim at the exit. Differently, the Euclidean map cannot interpret this phenomenon, as highlighted by the trajectories in Fig. 11.b. In this case, a simulated pedestrian using this distance map and starting close to a wall will walk to the exit touching the wall during the full path.

4. Model performance assessment

In this section, we provide some validation results by comparing the distance obtained by the proposed model and the distances observed in the calibration dataset in Section 4.1, while the result of simulations implementing the proposed distance map is illustrated in Section 4.2.

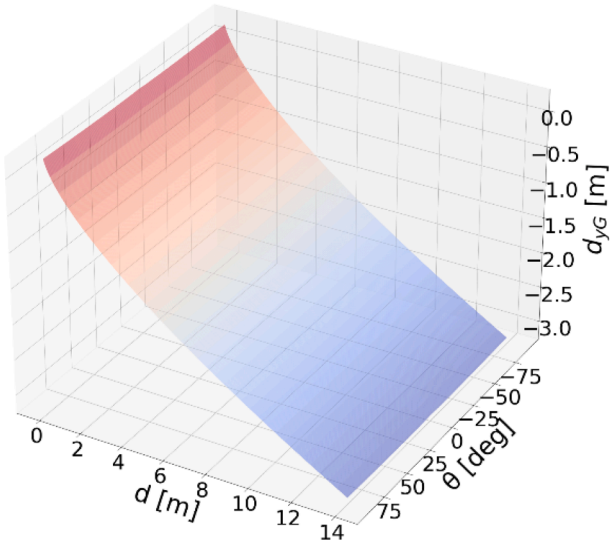

Fig. 10. d_{yG} representation function of d and θ in the model M6-U.

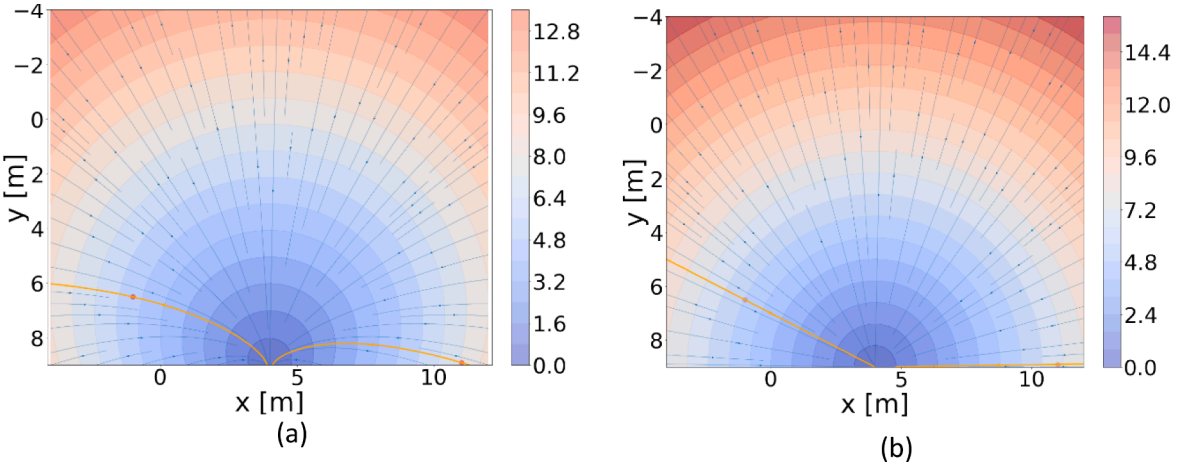

Fig. 11. Distance map and pedestrian trajectories for (a) the proposed distance map (b) the Euclidean distance map.

4.1. Distance comparison

First, is this initial part, we consider the effective walked distance by pedestrians as a metric to assess the performance of the model M4-U estimated. This performance is compared with the baseline model in Fig. 11.b, i.e., the traditional Euclidean distance map model used in the literature (Burstedde et al., 2001) (Kirchner & Schadschneider, 2002).

Fig. 12 shows a comparison between the real trajectories and the ones generated from the two distance maps compared in the case of the central exit: starting from the points in blue, the real data trajectories are in grey, while the ones generated by the distance maps in the same starting points are in orange. In this analysis, we only use real trajectories in which the tangents between the real trajectories and the distance map-based ones differ in the starting points less than $\phi = 30^{\circ}$: this allows us to filter out real trajectories in which the initial conditions (such as the entrance directly in the walkable space) strongly influence the full path of pedestrians. The plots in Fig. 12 clearly show how the trajectories by the proposed model (M4-U) are closer in terms of shapes to the real ones than the trajectories by the Euclidean model. This result is more evident for the real trajectories with y starting point coordinates greater than $y = 6\ m$.

We quantitively assess this evidence by considering the walked distance difference between the real trajectories and the simulated ones as a metric of similarity between the models and data (i.e., the difference between the grey and the orange trajectories in Fig. 12 expressed in meters). We consider two cases that include in the metrics computation: i) all the trajectories, ii) only trajectories with y starting point coordinate greater than $y = 6\ m$. This was done to assess how the different distance maps can predict the trajectories of people starting their walk close to the wall where the door is located.

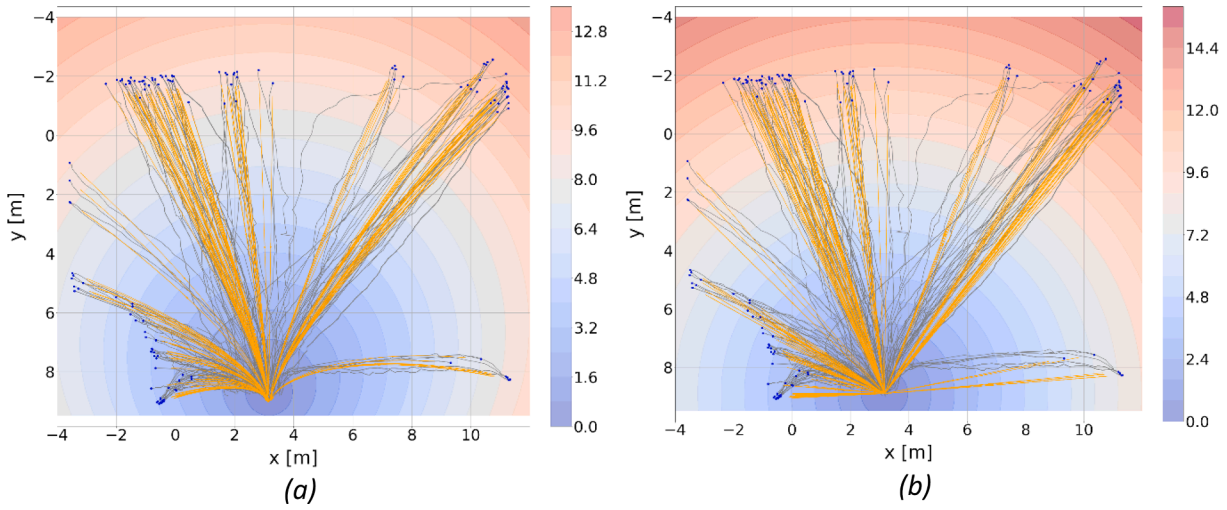

Fig. 12. Comparison between real trajectories and trajectories from distance maps in the case of the central exit. (a) M4-U; (b) Euclidean distance. The trajectories generated by the models are in orange, the real ones from data are in grey while the starting point of each trajectory is in blue. (For interpretation of the references to colour in this figure legend, the reader is referred to the web version of this article.)

Fig. 13 shows how much close the values of the walked distance obtained by the models are in comparison to the ground truth values of the real data. The red line represents the ideal condition in which the distances from the models perfectly match the real data; the more the blue points distribute close to the red line, the more the model can interpret the real data. The blue line represents instead the linear regression model fitting the real data to the predicted data, with the γ value representing its slope. By stating that the overlapping of these two lines is a measure of goodness for the models, we can affirm that the closer γ is to 45 deg, the better is the model fitting. By comparing (a) to (c) and (b) to (d) in Fig. 13 (and thus, in general, M4-U to the Euclidean model) by the γ values shown, it is evident that M4-U provide better performance in both the cases considered.

In line with the literature, we quantitatively measure the behaviour highlighted in Fig. 13. by reporting in Table 5 the computation of multiple metrics such as R^2 score, Mean Squared Error (MSE), Mean Absolute Error (MAE), Sum of Squares Due to Error (SSE), Sum of the Absolute Errors (SAE) and Round Mean Squared Error (RMSE) between the ground truth walked distances from the real trajectories and the ones obtained from the two models compared. The metrics in.

Table 5 clearly assess a better performance of M4-U on the baseline Euclidean model for both the cases considered.

4.2. Validation in a collective context

In all previous part, we only considered the case of (isolated) individuals walking toward a door. However, models using distance maps are typically employed in situations where a (large) number of people are moving toward an exit in a group. Since our distance map is calibrated using trajectories of individuals, it is possible that the model is over-calibrated for the scenario in which data were collected. Here, we wish, therefore, to check the potentials and limitations of the proposed model in a collective context where people need to exit from a room in a group and interactions between individuals also play an important role. First, we compare the proposed model with classical metrics used in traditional floor field cellular automaton models by benchmarking simulation results against experimental data collected in a laboratory experiment. Later, we study the property of our model in a collective condition by considering an imaginary scenario with a bigger number of people where it is easier to measure specific properties and grasp differences between our model and classical approaches.

To benchmark the proposed model, empirical data from an egress experiment are used here. The experiment has a very simple design. A mock-up room is created with cardboard delimiting the walls, and people are asked to leave the room after a start signal is given. The room was 4 m in width and 7 m in length, with the exit door being 80 cm wide and positioned in the middle of the longest side. Two different conditions were tested. In one condition, 25 people took part in the experiment and 3 repetitions were carried out. The second condition employed a higher initial density with 43 people; 5 repetitions were performed. Instructions were kept as simple as possible. Participants were simply asked to enter the room and leave from the exit at the "start" signal. For safety reasons, they were not allowed to run or push, and we simply asked them to avoid waiting too long in the same position.[5] A camera was set over the room to collect videos and extract participants' locations and trajectories (for details, see (Feliciani & Nishinari, 2018) (Feliciani & Nishinari, 2018)). An overview of the experiment is presented through some snapshots provided in Fig. 14. As seen, people typically occupied the room uniformly before egress started, although a sort of radial alignment can be observed.

[5] Sometimes participants in supervised experiments may wait in the corner and leave from the exit only when most people had already left. The instruction was intended to avoid this condition from happening and ensure a stable flow of people through the exit.

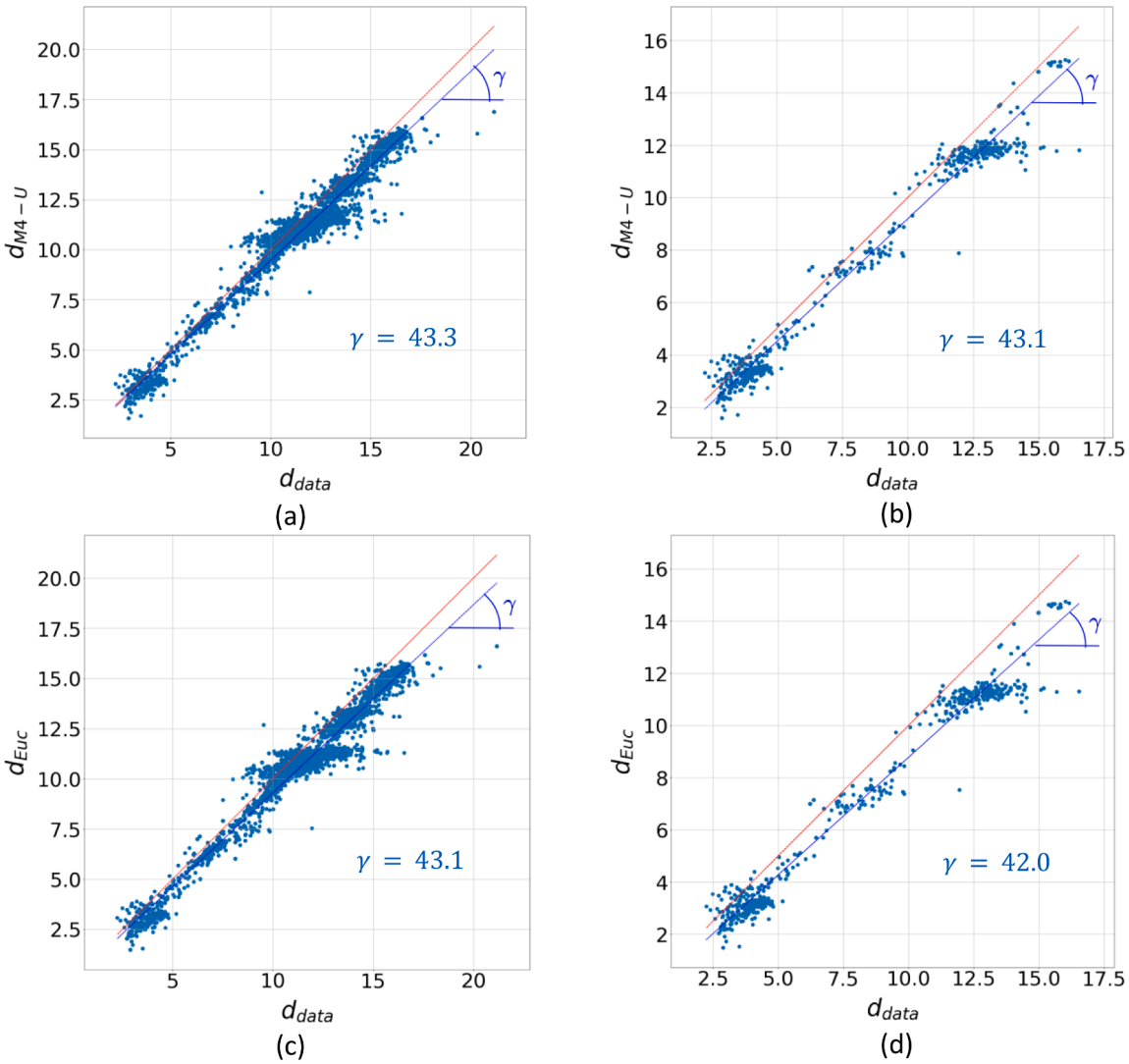

Fig. 13. Representation of the walked distances obtained with the models M4-U and Euclidean in comparison with the real walked distances from data. Two cases are considered: i) the whole dataset, where all the trajectories are used; ii) the filtered dataset, where only trajectories with the y coordinates of the starting point is greater than 6 m: (a) M4-U whole dataset, (b) M4-U filtered dataset, (c) Euclidean whole dataset, (d) Euclidean filtered dataset.

Table 5
Models' comparison based on multiple metrics.

Model	Trajectories considered	R^2	MSE	MAE	RMSE	SSE	SAE
Euclidean	All	0.87	1.01	0.85	1.00	9288.20	7442.94
	y > 6	0.89	1.76	1.12	1.33	2461.94	1531.97
M4-U	All	0.91	0.71	0.70	0.85	6624.35	5737.61
	y > 6	0.95	0.98	0.79	0.99	1376.39	1022.91

It is important to remark that experiments such as the ones reported here were performed by a number of researchers with a larger number of people and conditions close to emergency evacuation (see, for example, (Sieben et al., 2017) (Feliciani et al., 2020)). There are two main reasons why those specific experiments with 25 and 43 people are considered here. First, the authors are familiar with the experiments and this aspect plays a rather important role in laboratory experiments where instructions, the way they are given and what happened before, during, after the experiments can potentially influence the outcome. From this perspective the physical presence or a detailed documentation are necessary to understand the experiments and the context in which they are carried out. Second, they reproduce an egress situation which is in line with the data used to calibrate the model. In conditions close to emergency

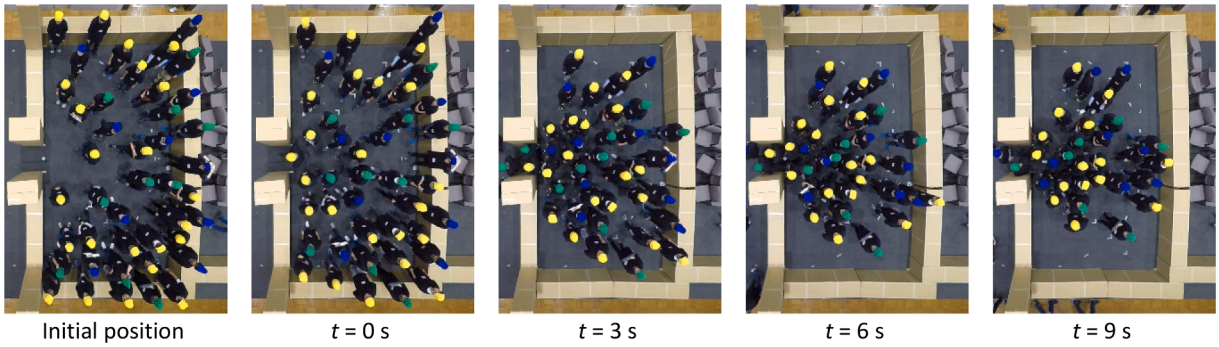

Fig. 14. Snapshot for the experiment with 43 participants. The scenario with 25 people is qualitatively similar, although, obviously, the initial density is lower. Time 0 s is set when the first person passes through the exit. Cap colour is used to codify different sensors attached to participants not used in this work (for details, see (Feliciani and Nishinari, 2018a).

evacuation, people are pushed toward the wall, and their behaviour is very different from the one being studied here, where we intended to reproduce people leaving space under normal conditions (leaving a school class, a concert, etc.).

To compare the modelling proposed here with classical approaches used in cellular automaton crowd simulation, we created a simple model with a Moore neighbourhood (the same used in calibrating the model as shown in Fig. 3) and where only the static Floor Field (distance map) is used. That means people move toward the exit only based on the static Floor Field and considering the occupancy of nearby cells. More specifically, the model is based on the following features, which are classical elements of cellular automaton models used for pedestrian dynamics.

- A cell size of 40 cm is used, which corresponds to the typical size of humans without external pressure. Different sizes were also used in previous studies, although 40 cm is arguably the most common selection.
- During each computational time step, pedestrians (which can occupy one cell at most) try to move to the cell having the highest probability associated to the Floor Field by using only empty cells in their neighbourhood. Since a single Floor Field is used, the distance map alone would be sufficient to determine a cell where people aim to move. However, for formalism Equation (3) is used to convert values of the Floor Field into probabilities.[6]
- If multiple neighbouring cells have the same probability (the distance map takes integer values to follow the discrete nature of CA), a cell is selected randomly among the multiple candidates.
- Positions are updated in parallel. This means that each pedestrian will select a position to move into the following time step, and if conflicts occur due to multiple people attempting to move into the same cell, only one is randomly selected.
- Free moving speed is the only parameter to be tuned, and it is used to compute the time step (by dividing cell size by walking speed). In this work, a speed of 0.90 m/s is used, which is in line to what found experimentally (when people walk through and slightly past the door). This value generally resulted in the best agreement with empirical egress time (details will follow). To account for the fact that diagonal cell-to-cell motion is $\sqrt{2}-1$ faster than a straight motion, the time step is artificially increased by $\frac{\sqrt{2}-1}{2}$ (assuming that half of the transitions occur diagonally). This is obviously a simplified assumption, but we deem it sufficient for the scope of model comparison and benchmarking.
- Exit is simulated using a single cell for accounting the fact that only one person can pass through the exit in each time step. This is clearly an approximation, since, as also shown in Fig. 14, two people may be able to align their bodies to use space more efficiently in reality (although this condition is rather rare, and usually, people would transit individually). But it is necessary to remember that the cellular automaton is a computational approach taking approximations in space and time, and assumptions are generally needed to translate reality into the simulation.

Using the floor field cellular automaton model with the rules presented above, three different distance maps were tested: the Manhattan and Euclidean distance metrics and the approach proposed here. More specifically, we will use model M4-U, which represents a good balance between simplicity and accuracy. The same geometry studied experimentally has been recreated in simulation, and the initial position of participants was employed in cellular automaton simulation used to minimise the differences between conditions studied in reality and numerical simulation. 10 repetitions were performed for each initial configuration tested experimentally, thus resulting in 30 repetitions for the low-density condition and 50 for the high-density condition.

The first indicator we study to evaluate the performance of the three distance map approaches is the egress time (defined as the time

[6] In calibrating the model k_S in the exponent of Equation (3) is used as a general parameter and the negative value is obtained through calibration. In short, the calibration process automatically infers that a negative value of k_S is needed to reproduce experimental data. In addition, in calibration k_S is dependent on several parameters and must be determined along with those parameters. In simulation, given that only the distance map determines the transition probabilities, a value of -1 is used.

Table 6
Numerical indicators are used to compare experimental results with numerical simulation using different distance map configurations. Egress time statistics are computed among trails for experiments and among repetitions for simulation. The density correlation coefficient (details formalised later in the text) is calculated on aggregate results andonly a single value is available for each condition. Crowd angle is provided for the whole crowd and for the left and right side in brackets, respectively (left first, right second). Note that since a weighted average is taken the total average may not be necessarily the mean between left and right side.

Measure (25 people)	Experiment	Manhattan	Euclidean	This work
Egress time (s)	18.52 ± 0.49	17.67 ± 1.46	17.44 ± 1.31	17.92 ± 1.26
Density correlation coefficient	1.000	0.655	0.577	0.724
Crowd angle (deg)	55.5 (51.3, 62.5)	41.1 (39.8, 42.6)	38.7 (38.1, 39.4)	45.9 (45.7, 46.0)
Measure (43 people)	**Experiment**	**Manhattan**	**Euclidean**	**This work**
Egress time (s)	29.90 ± 0.89	30.82 ± 1.71	30.79 ± 1.48	30.63 ± 1.81
Density correlation coefficient	1.000	0.829	0.816	0.888
Crowd angle (deg)	48.1 (45.7, 51.8)	40.1 (40.5, 39.8)	38.5 (38.6, 38.4)	45.1 (45.4, 44.8)

taken to empty the room after the first participant passes through the exit) presented in Table 6. In general, all models perform well in both low and high-density conditions. Moreover, we can notice that all models tend to underestimate egress time in the low-density condition and overestimate it in the high-density condition (with the model proposed here performing slightly better). However, a good result regarding egress time was to be expected since free speed was calibrated to match experimental results. Also, egress time does not say much on the accuracy of a model since it represents only a simple value providing no indication of space utilisation within the room.

In that sense, the average occupancy of each cell can be used to compute the density distribution, which can be easily compared with experimental data, with results presented in Fig. 15. From the density heatmaps presented in Fig. 15 the differences between the three models become clearer. In particular, because of the settings used in defining the distance to the exit, the Manhattan approach results in a triangular shape, which is very different to what was observed experimentally. The Euclidean approach and the model proposed here show similar profiles, although our model generally depicts better the tendency of avoiding the walls (see also Fig. 14).

To quantify the accuracy of each approach as presented by the density profiles, we computed the correlation coefficients between experimental and simulation by comparing values in each cell with the outcome reported in Table 6. Results show that regardless of the initial density, our distance map outperforms the classical approaches used in the model implementation. However, this could be due to numerical artefacts associated with using the correlation coefficient (designed for 1D series) in a 2D context.

To better measure some features of the density maps in the context considered here, we therefore additionally introduce the "crowd angle" defined by Equation (8):

$$\beta = \frac{\sum_{area} \operatorname{atan}\left(\frac{dy(i,j)}{dx(i,j)}\right) \bullet \rho(\mathrm{i},\mathrm{j})}{\sum_{area} \rho(\mathrm{i},\mathrm{j})} \tag{8}$$

where $dx(i,j)$ and $dy(i,j)$ are the distances from cell (i,j) to the exit and $\rho(i,j)$ the local density in that position.[7] The calculation is performed on the left and right half of the room with respect to the exit, with the average between both sides taken. The crowd angle allows providing a first-hand approximation of the shape collectively formed by the group leaving the room. Values close to 0° indicate a tendency to stay close to the wall, while values close to 90° are obtained when people line up in an ordinate manner. The crowd angle for the three distance map configurations is presented in Table 6, showing that, also under this perspective, the model presented here achieves results closer to the experimental case, especially in the condition with 43 participants. The better performance for the more crowded condition can be also explained by the more organized orientation of the participants. In fact, whereas the condition with 25 participants shows large differences between the left and right side, the high-density condition is more symmetric and less dependent on the initial position of the participants.

The experiments considered above are useful to benchmark the proposed model and confirm that its features are in line with human behaviour observed empirically. However, the low number of participants makes it difficult to grasp the differences between the proposed model here and classical geometries. We will, therefore, also consider a room 50 × 50 cells in size (20 m if a cell of 0.4 m is considered) with an initial occupancy of 500 people. Such a setting would be difficult to reproduce in controlled experiments but can be easily set up in simulation. In this case, given the larger room, a two cells exit is assumed.

Results obtained using this larger room are presented in Fig. 16. Representative frames were taken from the simulation to qualitatively show the features of the proposed model. As Fig. 16 shows, although the crowd takes a generally round shape, the largest width is observed slightly away from the wall (especially in time step 120). In contrast, in the Euclidean approach, the largest number of people is amassed at the walls, which is typically not observed in normal egress conditions.

To further analyse the results, the temporal evolution of crowd angle was computed using people positions instead of the density indicated in Equation (8) (0 for empty cells and 1 for occupied cells). Results are presented in Fig. 17. The initial increase is created by

[7] Equation (8) is no less than a weighted average of the angle taken by the crowd in each half of the room with local density representing the weights. The name "crowd angle" is simply used as it represents a more intuitive and shorter expression and "weighted average angle.".

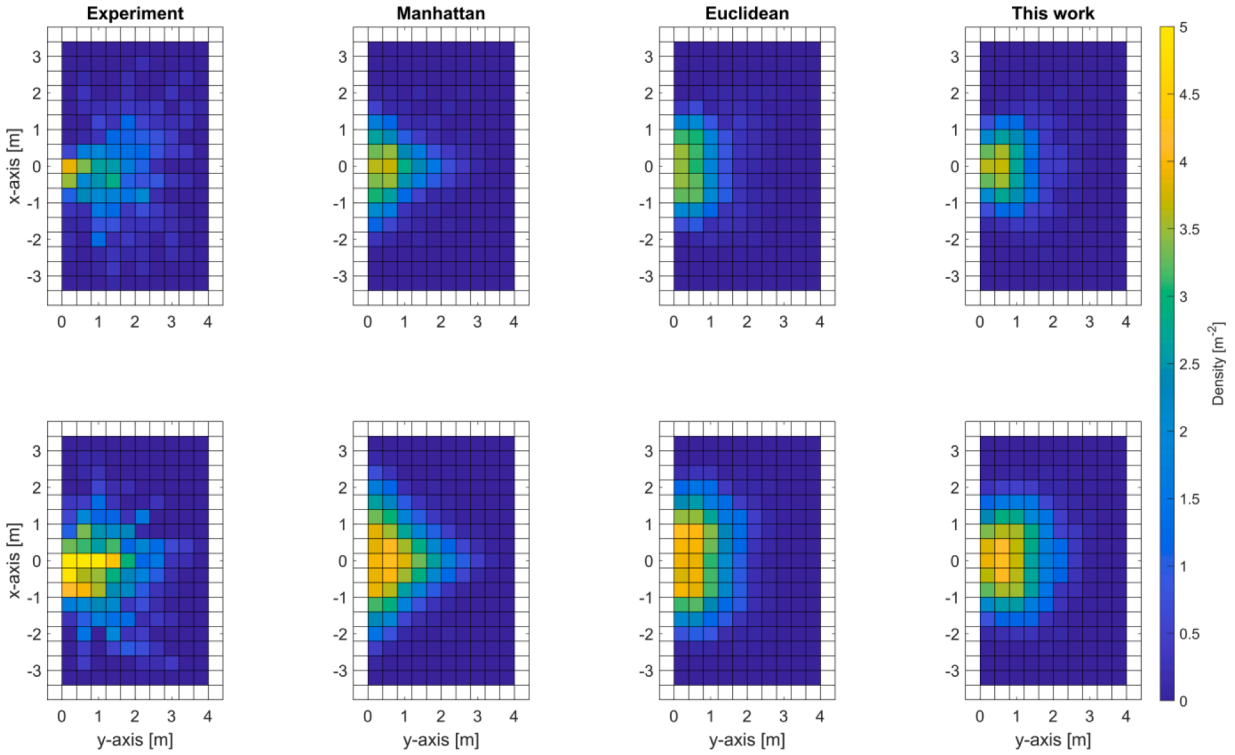

Fig. 15. Average density recorded in each position (or cell) in the time period relative to the first participant passing through the exit until the last one leaving the door. The upper row is relative to the low-density condition with 25 participants, the lower row to the condition with 43 people. Cell size is 0.4 m in width. Exit is located at (0,0).

the people being randomly distributed inside the room and moving toward the exit. But after 10 s, the differences among the distance maps emerge clearly. The Euclidean geometry converges toward a 45° configuration as people dispose radially. On the other hand, the elongated "queue" created by the Manhattan approach results in high angles. The approach presented here can be seen as a trade-off showing that people do tend to "queue", but, at the same time, they also attempt to leave the room in directions parallel to the walls.

To conclude this section, we wish to briefly comment on the validity of our model for highly competitive scenarios. As already stated, the model has been tested, calibrated and was purposedly validated using non-competitive conditions. Further, experimental data available for very competitive conditions (see for example (Feliciani et al., 2020) or (Sieben et al., 2017)) usually do not cover the whole crowd (especially in the early stages of evacuation), thus making it difficult to obtain accurate density maps or compute the crowd angle. It is nonetheless interesting that, even in very competitive conditions, the shape taken by the crowd appear to be a circle with the centre slightly shifted from the exit toward the room. This can be observed from the videos provided in (Garcimartín et al., 2013) and (Garcimartín et al., 2017), and partially through the density maps shown in (Feliciani et al., 2020). This aspect clearly deserves a deeper and ad-hoc investigation, but it is possible that even in competitive conditions people avoid the area close to the wall, possibly for reasons not necessarily similar to the ones used to explain the behaviour upon which this work was based.

5. Discussion and conclusions

In this work, we investigate how pedestrians navigate in spaces without obstacles and how this can be formalised in terms of a distance map model. This was achieved by challenging the static goal assumption adopted by the traditional pedestrian models, in which pedestrians aim at the central location of an exit or its other geometrical features (Chraibi et al., 2013) during the full movement toward it. To the best of our knowledge, this work represents the first attempt to challenge this assumption. Thus, we proposed a conceptual model in Section 2.1, assuming a changing pedestrians' goal depending on their location with respect to the exit they are aiming at. In this investigation, we started by hypothesizing the moving goal for the pedestrians during their exit from a room. Then, we verified on real data that this assumption provided better results than traditional CA models. We then noticed another interesting feature of the model: without adding any further wall-repulsion component, the proposed distance map guided people through curved trajectories toward the goal.

To test the proposed conceptual model, we use 9000 trajectories filtered to form the pedestrian dataset by Majecka et al. (Majecka, 2009) and different nested model specifications (12 models in Table 1 and Fig. 2) assuming the change of pedestrian goal as a function of d and θ, which are defined in Fig. 1. The results in Section 3.1 show that the distance of a pedestrian from an exit is the main variable affecting the distance map. Fig. 6 clearly indicates that pedestrians head for goals in front of the exit when their distance from it is

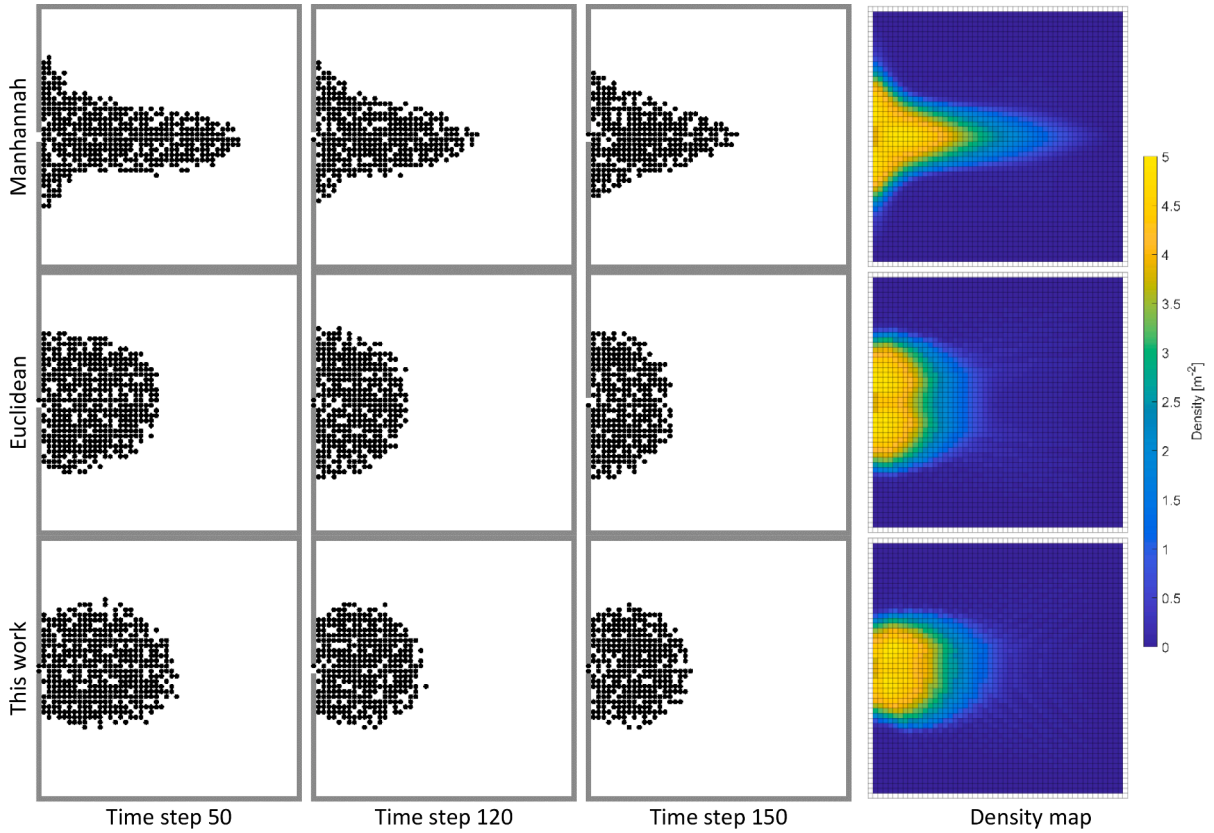

Fig. 16. Frames taken during simulation using different distance maps (left) and final density map (right). A room having a size of 50 × 50 is taken as an example and 500 people are randomly placed inside it as the initial configuration. 100 repetitions were used to generate the average density map presented on the right.

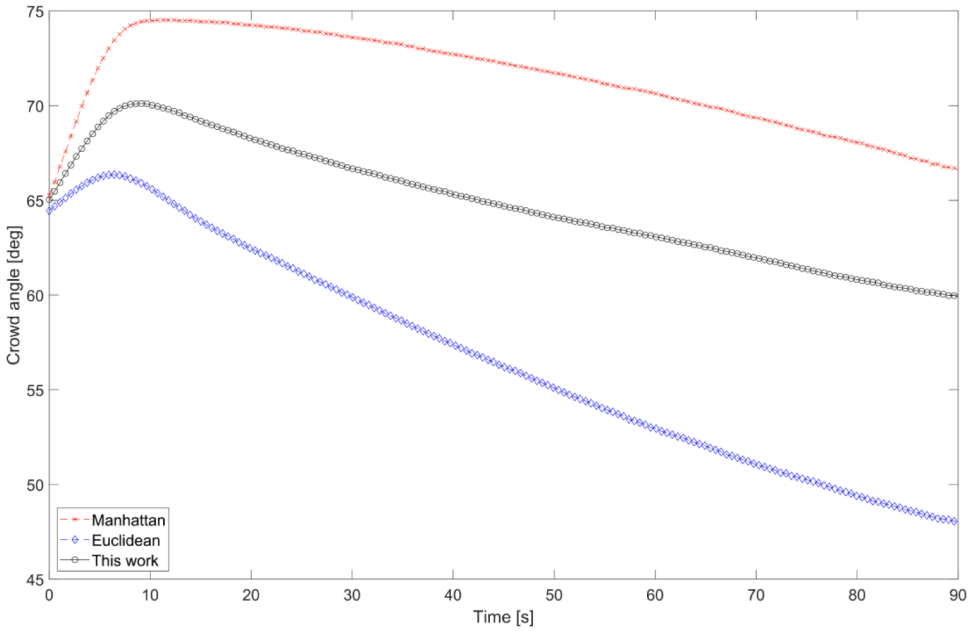

Fig. 17. Crowd angle computed using the geometry of Fig. 17 and averaged from 100 repetitions.

greater than 0.5 m while their actual goal is beyond the center of the exit for shorter distances. Although the results in Section 3.1 indicate that θ also has an impact on the distance map, the results in Section 3.2 provide evidence that the impact of θ is minimal and can be ignored. This led us to select the MU-4 (Table 1) as the best model specification describing the phenomenon under investigation by following the parsimony modelling principle. This feature makes the model easier to be implemented in existing and new pedestrian and evacuation software tools (Lovreglio et al., 2019). In fact, the distance map could be used in its original form for discrete models such as the floor field cellular automata model, or it is gradient can be used to define the desired direction field (Burstedde et al., 2001) (Kirchner & Schadschneider, 2002) for the continuous model as the social force model (Moussaïd et al., 2011).

The open dataset (Majecka, 2009) used in this work was selected due to its high ecological validity. In fact, the movement of thousands of pedestrians was recorded in an open space environment during the building's operative conditions. As such, unlike in many laboratory experiments, the pedestrian was not affected by any other conditions, and they displayed their true behaviour. Although laboratory experiments can reach thousands of trajectories, these are generally coming from a very limited sample size of participants who are asked to perform different walking and evacuating tasks multiple times. Differently, in the selected dataset, the trajectories are from more building occupants showing a more heterogeneous behaviour in their walking patterns. These filtered trajectories used in this investigation were collected in a built environment scenarios having multiple exits on the same wall. This feature might have some impact on the results proposed in this work. However, this is a common feature in many large empty indoor spaces, such as atrium, and this dataset was selected given its unique combination of sample size and ecological validity. Finally, we believe that if there is any impact, its effect is marginal as dataset shows similar curvatures of pedestrian which do not use the one of the other doors on the same wall of the exit as starting point as shown in Fig. 5. Further, the use of big data has implications for how the parameters of the calibrated model can be interpreted. In fact, all the p-values of the parameters are below the 0.01 threshold, but this does not imply that all the factors investigated in the model can have a meaningful impact on the description of the phenomenon (Ioannidis, 2019). As such, we use a sensitivity analysis to highlight the impact of the two factors under investigation in this work.

The main contribution is the proposal of an innovative modelling solution in which we assume a moving goal which pedestrians head for while moving. Based on this assumption, we specify and calibrate a new distance map using real data. The proposed distance map performs better if compared to traditional distance maps (such as Eulerian one) and features an important characteristic, i.e., the capability to originate curved trajectories for pedestrians' movement toward their goals. Moreover, we tested our distance maps in scenarios and applications different from the set-up on which it was calibrated (i.e. evacuation context in section 4.2). The metrics measured in these scenarios confirmed that the proposed map perform better than traditional maps.

A key feature of the proposed model is its capability to have pedestrian walking away from walls, as shown in Fig. 12.a. This feature is in line with what is observed in many previous pedestrian studies, and it is considered by fire engineers when calculating the effective design width of an enclosed environment with walls and obstacles (Gwynne & Rosenbaum, 2016) (Purser, 2010) (Graat et al., 1999) (Ronchi et al., 2014). According to the latest SFPE handbook, the boundary layer width accounting for the unused space by pedestrians can vary from 9 cm to 46 cm, which is the same order of magnitude we can observe in the trajectory drawn in Fig. 12.a (See Table 5 9.1 in (Gwynne & Rosenbaum, 2016)). This feature is not available in traditional models using Euclidean distance metrics as distance maps (Burstedde et al., 2001) (Kirchner & Schadschneider, 2002) or the latest more advanced data-driven metrics proposed by Lovreglio et al. (Lovreglio et al., 2018). In fact, the proposed deforming the Euclidean matrix in (Lovreglio et al., 2018) generate trajectories almost parallel to the wall when a pedestrian is away from an exit and close to the same wall; these trajectories start curving when the pedestrian is a few meters away from the door (please refer to Fig. 8 of the referenced paper: link). In other words, deformed Euclidean matrix can partially mimic the behaviour of pedestrian while not investigating the true reason behind these curved trajectories. On the other hand, having the possibility to change the pedestrian goal as a function of the distance allows the distance maps to achieve modelling solution closer to the observed trajectories in Fig. 5, as well as provide evidence on the reason behind these curvatures.

The proposed distance map has been tested in this work using two different approaches (see Section 4). In the first approach, we compared the actual distances walked by the building occupants in the calibration dataset with the distances generated by the proposed distance map and the traditional Euclidean distance map. The results clearly show how the features in Fig. 11 have strong implications in terms of distances. In fact, the results in Table 5 show that the simulated distances from the proposed distance map clearly outperforms the results of the Euclidean map, especially for agents starting their path close to the wall where the door is located. Finally, we tested the proposed distance map against a pedestrian dataset published in (Feliciani & Nishinari, 2018) (Feliciani & Nishinari, 2018) by implementing the distance map in a floor field cellular automaton model. This validation exercise also shows that the proposed distance map provides better results than traditional maps in terms of densities and the crowd angle matrix proposed in Equation (8).

In this work, we tested the proposed distance map using CA models. In the related simulations, the evacuation interactions were modelled using simple rules proposed in (Burstedde et al., 2001). However, future implementation can integrate the proposed map with more advanced evacuees' interaction rules. Further, as explained in the Introduction, a distance map can be converted into a vector field by normalising the gradient of the distance map, as illustrated in Footnote 1 of this paper. The derived vector field can be used in continuous social force models as the desired direction for evacuees.

One limitation is that this paper only uses trajectory data without considering the actual biomechanics of pedestrians focusing on features like their steps length, body rotation etc. This represents a new trend in the pedestrian and evacuation dynamic field (Agyemang & Kinateder, 2022) (Ronchi et al., 2019) (Zanlungo et al., 2023). However, existing open datasets providing the full body posture of a pedestrian while evacuating or existing doors are still not available, and they will require a completely new approach to model and analyse pedestrian navigation. As such, this work relies on the use of traditional trajectories tracking the full body of a pedestrian as a point in a two-dimensional space using the assumption described in (Majecka, 2009).

The paper does not investigate the potential contribution of further modelling components such as translational inertia, rotational inertia, and repulsion from walls. Even if the model proposed shows good performance, there is still space for improvement which can be driven by considering these components' contribution. This further investigation requires dealing not only with trajectories (thus, with spatial features of the pedestrians) but also with time-related quantities (such as speeds): there is a clear need for quantifying the trade-off between model complexity and efficacy. This evaluation can be conducted in future works by investigating the comparison between the model proposed and the class of CA models integrating the repulsion from walls component (Nishinari et al., 2004). Despite sharing the peculiarity of interpreting curved trajectories, the hypothesis driving this feature is quite different: the model presented exploits the moving-goal hypothesis, while the other models some mechanistic rules derived from the Social Force Model. This further investigation can potentially expand the behavioural comprehension of the pedestrian dynamics. We state that this work is interpretable as a further behavioural layer implementable on static distance map-based models.

Another limitation of this work is that we assumed uniform behaviour among all the observed pedestrians. As such, the model proposed in this work provides an average trend for the full sample available for calibration. The lack of heterogeneities can be overcome in future studies by assessing how different demographics might affect the goals of pedestrians as they approach an exit as well as using random-parameter models or Bayesian-based models following the trend observed for exit choice investigations (Lovreglio et al., 2016) (Song & Lovreglio, 2021). However, the used dataset does not provide this information, and it was not possible to test different demographics-related assumptions. Another possible path to account for heterogeneity could be the use of the Random Parameter Model (also known as mixed models) or the use of the Hierarchical Bayes Estimator (Song & Lovreglio, 2021) to identify differences among the observed pedestrians.

CRediT authorship contribution statement

Parisi Fabio: Conceptualization, Methodology, Software, Formal analysis, Investigation, Writing – original draft, Writing – review & editing. **Feliciani Claudio:** Methodology, Formal analysis, Validation, Writing – original draft, Writing – review & editing. **Lovreglio Ruggiero:** Conceptualization, Methodology, Investigation, Writing – original draft, Writing – review & editing, Funding acquisition.

Declaration of Competing Interest

The authors declare that they have no known competing financial interests or personal relationships that could have appeared to influence the work reported in this paper.

Acknowledgements

Part of this work was financially supported by the JST-Mirai Program Grant Number JPMJMI20D1 and the JSPS KAKENHI Grant Number JP23K13521. The authors would like to acknowledge the School of Built Environment (Massey University) for supporting the visiting expenses of Dr Fabio Parisi in 2022. The authors thank Father Mer Duffy (Te Kupenga - Catholic Theological College) for the insightful suggestion on the conceptual modelling solution.

References

Agyemang, C., Kinateder, M., 2022. A review of the biomechanics of staircase descent: implications for building fire evacuations. Fire Technol. Volume 58, 379–413. https://doi.org/10.1007/S10694-021-01140-Y/TABLES/3, 1 1.

Alizadeh, R., 2011. A dynamic cellular automaton model for evacuation process with obstacles. Saf. Sci. Volume 49, 315–323. https://doi.org/10.1016/j.ssci.2010.09.006, 2.

Anvari, B., Bell, M.G.H., Sivakumar, A., Ochieng, W.Y., 2015. Modelling shared space users via rule-based social force model. Transportation Research Part C: Emerging Technologies Volume 51, 83–103. https://doi.org/10.1016/J.TRC.2014.10.012, 1 2.

Bierlaire, M., 2020. A short introduction to PandasBiogeme, 2020. https://transp-or.epfl.ch/documents/technicalreports/bier20.pdf.

Burstedde, C., Klauck, K., Schadschneider, A., Zittartz, J., 2001. Simulation of pedestrian dynamics using a two-dimensional cellular automaton. Physica A: Statistical Mechanics and its Applications Volume 295, 507–525. https://doi.org/10.1016/S0378-4371(01)00141-8, 6.

Cerwick, D.M., Gkritza, K., Shaheed, M.S., Hans, Z., 2014. A comparison of the mixed logit and latent class methods for crash severity analysis. Analytic Methods in Accident Research Volume 3–4, 11–27. https://doi.org/10.1016/J.AMAR.2014.09.002, 1 10.

Chraibi, M., Freialdenhoven, M., Schadschneider, A., Seyfried, A., 2013. Modeling the desired direction in a force-based model for pedestrian dynamics. Traffic and Granular Flow '11, 263–275. https://doi.org/10.1007/978-3-642-39669-4_25.

Corbetta, A., Muntean, A., Vafayi, K., 2015. Parameter estimation of social forces in pedestrian dynamics models via a probabilistic method. Math. Biosci. Eng. Volume 12, 337–356. https://doi.org/10.3934/MBE.2015.12.337, 1 4.

Dias, C., Lovreglio, R., 2018. Calibrating cellular automaton models for pedestrians walking through corners. Physics Letters, Section A: General, Atomic and Solid State Physics. 382 (19), 1255–1261. https://doi.org/10.1016/j.physleta.2018.03.022.

Duives, D.C., Daamen, W., Hoogendoorn, S.P., 2013. State-of-the-art crowd motion simulation models. Transportation Research Part C: Emerging Technologies Volume 37, 193–209. https://doi.org/10.1016/J.TRC.2013.02.005, 1 12.

Feliciani, C., Zuriguel, I., Garcimartín, A., Maza, D. & Nischinari, K., 2020. Systematic experimental investigation of the obstacle effect during non-competitive and extremely competitive evacuations. *Scientific Reports 2020 10:1,* 29 9, Volume 10, p. 1–20. https://doi.org/10.1038/s41598-020-72733-w.

Feliciani, C., Nishinari, K., 2018a. Estimation of pedestrian crowds' properties using commercial tablets and smartphones. Transportmetrica B: transport dynamics Volume 7, 865–896. https://doi.org/10.1080/21680566.2018.1517061, 23 12.

Feliciani, C., Nishinari, K., 2018b. Measurement of congestion and intrinsic risk in pedestrian crowds. Transportation Research Part C: Emerging Technologies Volume 91, 124–155. https://doi.org/10.1016/J.TRC.2018.03.027, 1 6.

Feng, Y., Duives, D., Daamen, W., Hoogendoorn, S., 2021. Data collection methods for studying pedestrian behaviour: A systematic review. Build. Environ. Volume 187, 107329 https://doi.org/10.1016/J.BUILDENV.2020.107329, 1 1.

Fu, Z., Jia, Q., Chen, J., Ma, J., Han, K., Luo, L., 2018. A fine discrete field cellular automaton for pedestrian dynamics integrating pedestrian heterogeneity, anisotropy, and time-dependent characteristics. Transportation Research Part C: Emerging Technologies Volume 91, 37–61. https://doi.org/10.1016/J.TRC.2018.03.022, 1 6.

Garcimartín, A., Pastor, J.M., Martín-Gómez, C., Parisi, D. & Zuriguel, I., 2013. Evacuation through a narrow door. [Online] Available at: https://ped.fz-juelich.de/da/doku.php?id=evacuation_narrow_door, https://doi.org/10.34735/ped.2013.9 (accessed July 20, 2023).

Garcimartín, A., Zuriguel, I., Maza, D., Pastor, J.M., Parisi, D. & Martín-Gómez, C., 2017. Evacuation through a narrow door in the presence of an obstacle. [Online] Available at: https://ped.fz-juelich.de/da/doku.php?id=evacuation_narrow_door_obstacle, https://doi.org/10.34735/ped.2017.3 (accessed July 20, 2023).

Graat, E., Midden, C., Bockholts, P., 1999. Complex evacuation; effects of motivation level and slope of stairs on emergency egress time in a sports stadium. Saf. Sci. Volume 31, 127–141. https://doi.org/10.1016/S0925-7535(98)00061-7, 1 3.

Greene, W.H., 2011. Econometric Analysis -, 7th Edition. Pearson, London(UK).

Guo, R.Y., Huang, H.J., 2012. Formulation of pedestrian movement in microscopic models with continuous space representation. Transportation Research Part C: Emerging Technologies Volume 24, 50–61. https://doi.org/10.1016/J.TRC.2012.02.004, 1 10.

Gwynne, V. S. M. & Rosenbaum, E. R., 2016. Employing the Hydraulic Model in Assessing Emergency Movement. In: *SFPE Handbook of Fire Protection Engineering.* New (York): Springer New York, p. 2115–2151.https://doi.org/10.1007/978-1-4939-2565-0_59.

Haghani, M., 2020a. Empirical methods in pedestrian, crowd and evacuation dynamics: Part I. Experimental methods and emerging topics. Saf. Sci. 129, 104743 https://doi.org/10.1016/J.SSCI.2020.104743.

Haghani, M., 2020b. Empirical methods in pedestrian, crowd and evacuation dynamics: Part II. Field methods and controversial topics. Saf. Sci. Volume 129, 104760 https://doi.org/10.1016/J.SSCI.2020.104760, 1 9.

Haghani, M., Lovreglio, R., 2022. Data-based tools can prevent crowd crushes. Science 378, 1060–1061. https://doi.org/10.1126/SCIENCE.ADF5949.

Haghani, M., Sarvi, M., 2018. Crowd behaviour and motion: Empirical methods. Transp. Res. B Methodol. Volume 107, 253–294. https://doi.org/10.1016/J.TRB.2017.06.017, 1 1.

Hänseler, F.S., Lam, W.H.K., Bierlaire, M., Lederrey, G., Nikolić, M., 2017. A dynamic network loading model for anisotropic and congested pedestrian flows. Transp. Res. B Methodol. 95, 149–168. https://doi.org/10.1016/J.TRB.2016.10.017.

Helbing, D., Farkas, I., Vicsek, T., 2000. Simulating dynamical features of escape panic. Nature Volume 407, 487–490. https://doi.org/10.1038/35035023, 28 9.

Hensher, D. A., Rose, J. M. & Greene, W. H., 2005. *Applied Choice Analysis: A Primer.* , Cambridge University Press, 2005.

Hess, S., Palma, D., 2019. Apollo: A flexible, powerful and customisable freeware package for choice model estimation and application. Journal of Choice Modelling Volume 32, 100170. https://doi.org/10.1016/J.JOCM.2019.100170, 1 9.

Hoogendoorn, S., Bovy, P., 2004. Pedestrian route-choice and activity scheduling theory and models. Transp. Res. Part B Methodol 38, 169–190. https://doi.org/10.1016/S0191-2615(03)00007-9.

Hsu, J.J., Chu, J.C., 2014. Long-term congestion anticipation and aversion in pedestrian simulation using floor field cellular automata. Transportation Research Part C: Emerging Technologies Volume 48, 195–211. https://doi.org/10.1016/j.trc.2014.08.021, 11.

Huang, R., Zhao, X., Zhou, C., Kong, L., Liu, C., Yu, Q., 2022. Static floor field construction and fine discrete cellular automaton model: Algorithms, simulations and insights. Physica A: Statistical Mechanics and its Applications Volume 606, 128150. https://doi.org/10.1016/J.PHYSA.2022.128150, 15 11.

Ioannidis, J.P.A., 2019. What have we (Not) learnt from millions of scientific papers with P values? Am. Stat. Volume 73, 20–25, 29 3.

Johansson, A., Batty, M., Hayashi, K., Al Bar, O., Marcozzi, D., Memish, Z.A., 2012. Crowd and environmental management during mass gatherings. Lancet Infect. Dis. Volume 12, 150–156. https://doi.org/10.1016/S1473-3099(11)70287-0, 1 2.

Karmakharm, T., Richmond, P. & Romano, D. M., 2010. Agent-based large scale simulation of pedestrians with adaptive realistic navigation vector fields. *Theory and Practice of Computer Graphics 2010, TPCG 2010 - Eurographics UK Chapter Proceedings,* p. 67–74. https://doi.org/10.2312/LOCALCHAPTEREVENTS/TPCG/TPCG10/067-074.

Kirchner, A., Schadschneider, A., 2002. Simulation of evacuation processes using a bionics-inspired cellular automaton model for pedestrian dynamics. Physica A: Statistical Mechanics and its Applications Volume 312, 1–19. https://doi.org/10.1016/S0378-4371(02)00857-9, 9.

Korhonen, T., 2017. *Fire Dynamics Simulator with Evacuation: FDS+Evac - VTT Technical Reference and User's Guide.* http://virtual.vtt.fi/virtual/proj6/fdsevac/documents/FDS+EVAC_Guide.pdf (accessed June 28, 2023).

Kretz, T., Große, A., Hengst, S., Kautzsch, L., Pohlmann, A., Vortisch, P., 2011. Quickest Paths In Simulations Of Pedestrians. Advances in Complex Systems Volume 14, 733–759. https://doi.org/10.1142/S0219525911003281, 20 11.

Kuligowski, E. D., Peacock, R. D. & Hoskins, B. L., 2010. *A Review of Building Evacuation Models, 2nd Edition-Technical Note (NIST TN) - 1680,* Gaithersburg: s.n.

Kuligowski, E. D., 2016. Computer Evacuation Models for Buildings. In: *SFPE Handbook of Fire Protection Engineering.* In: *SFPE Handbook of Fire Protection Engineering.* New(York): Springer New York, p. 2152–2180.

Lenoir, M., Van Overschelde, S., De Rycke, M., Musch, E., 2006. Intrinsic and extrinsic factors of turning preferences in humans. Neurosci. Lett. 393 (2–3), 179–183.

Li, Y., Chen, M., Dou, Z., Zheng, X., Cheng, Y., Mebarki, A., 2019. A review of cellular automata models for crowd evacuation. Physica A: Statistical Mechanics and its Applications Volume 526, 120752. https://doi.org/10.1016/J.PHYSA.2019.03.117, 15 7.

Lovreglio, R., Dias, C., Xiang, S. & Ballerini, L., 2017. *Towards Microscopic Calibration of Pedestrian Simulation Models using Open Trajectory Datasets: the Case Study of the Edinburgh Informatics Forum,* In: Conf. Traffic Granul. Flow 2017, 2017.

Lovreglio, R., Ronchi, E., Nilsson, D., 2015. Calibrating floor field cellular automaton models for pedestrian dynamics by using likelihood function optimization. Physica A: Statistical Mechanics and its Applications 438, 308–320. https://doi.org/10.1016/j.physa.2015.06.040.

Lovreglio, R., Dias, C., Song, X., Ballerini, L., 2018. Investigating Pedestrian Navigation in Indoor Open Space Environments Using Big Data. Applied Mathematical Modelling. https://doi.org/10.1016/j.apm.2018.06.014.

Lovreglio, R., Fonzone, A., Dell'Olio, L., 2016. A mixed logit model for predicting exit choice during building evacuations. Transp. Res. A 92, 59–75.

Lovreglio, R., Dia, C., Song, X., Ballerini, L., 2018. Investigating pedestrian navigation in indoor open space environments using big data. App. Math. Model. 62, 499–509. https://doi.org/10.1016/j.apm.2018.06.014.

Lovreglio, R., Ronchi, E., Kinsey, M.J., 2019. An online survey of pedestrian evacuation model usage and users. Fire Technol. Volume 56, 1133–1153. https://doi.org/10.1007/s10694-019-00923-8, 5 11.

Lu, L., Chan, C.Y., Wang, J., Wang, W., 2017. A study of pedestrian group behaviors in crowd evacuation based on an extended floor field cellular automaton model. Transportation Research Part C: Emerging Technologies Volume 81, 317–329. https://doi.org/10.1016/J.TRC.2016.08.018, 1 8.

Majecka, B., 2009. *Statistical models of pedestrian behaviour in the forum,* 2009. https://citeseerx.ist.psu.edu/document?repid=rep1&type=pdf&doi=6505d259758fc2fd4e60da018c35d687a2ddc250 (accessed June 28, 2023).

Molloy, J., Becker, F., Schmid, B., Axhausen, K.W., 2021. mixl: An open-source R package for estimating complex choice models on large datasets. Journal of Choice Modelling Volume 39, 100284. https://doi.org/10.1016/J.JOCM.2021.100284, 1 6.

Moussaïd, M., Helbing, D., Theraulaz, G., 2011. How simple rules determine pedestrian behavior and crowd disasters. Proc. Natl. Acad. Sci. U.S.A. 108 (17), 6884–6888.

Moustaid, E., Flötteröd, G., 2021. Macroscopic model of multidirectional pedestrian network flows. Transp. Res. B Methodol. Volume 145, 1–23. https://doi.org/10.1016/J.TRB.2020.12.004, 1 3.

Nishinari, K., Kirchner, A., Namazi, A. & Schadschneider, A., 2004. Extended Floor Field CA Model for Evacuation Dynamics. *IEICE TRANSACTIONS on Information and Systems,* 1 3, Volume E87-D, p. 726–732. http://search.ieice.org/bin/summary.php?id=e87-d_3_726&category=D&year=2004&lang=E&abst= (accessed January 15, 2015).

Purser, D., 2010. Dependence of Modelled Evacuation Times on Key Parameters and Interactions. Pedestrian and Evacuation Dynamics 2008, 667–675. https://doi.org/10.1007/978-3-642-04504-2_63.

Ronchi, E., Kuligowski, E.D., Peacock, R.D., Reneke, P.A., 2014. A probabilistic approach for the analysis of evacuation movement data. Fire Saf. J. Volume 63, 69–78. https://doi.org/10.1016/J.FIRESAF.2013.11.012, 1 1.

Ronchi, E., Corbetta, A., Galea, E.R., Kinateder, M., Kuligowski, E., McGrath, D., Pel, A., Shiban, Y., Thompson, P., Toschi, F., 2019. New approaches to evacuation modelling for fire safety engineering applications. Fire Saf. J. Volume 106, 197–209. https://doi.org/10.1016/J.FIRESAF.2019.05.002, 1 6.

Shen, J., 2009. Latent class model or mixed logit model? A comparison by transport mode choice data. Appl. Econ. 41 (22), 2915–2924. https://doi.org/10.1080/00036840801964633.

Sieben, A., Schumann, J., Seyfried, A., Chialvo, D.R., 2017. Collective phenomena in crowds—Where pedestrian dynamics need social psychology. PLoS One 12 (6), e0177328. https://doi.org/10.1371/JOURNAL.PONE.0177328.

Song, B.X., Lovreglio, R., 2021. Investigating personalized exit choice behavior in fire accidents using the hierarchical Bayes estimator of the random coefficient logit model. Analytic Methods in Accident Research Volume 29, 100140. https://doi.org/10.1016/J.AMAR.2020.100140, 1 3.

Souman, J.L., Frissen, I., Sreenivasa, M.N., Ernst, M.O., 2009. Walking straight into circles. Curr. Biol. 19 (18), 1538–1542.

Steffen, B. & Seyfried, A., 2009. Modelling of pedestrian movement around 90 and 180 bends, in: Adv. Res. Work. Fire Prot. Life Saf. Build. Transp. Syst.. https://www.researchgate.net/profile/Armin-Seyfried/publication/45887941_Modeling_of_pedestrian_movement_around_90_and_180_degree_bends/links/62bee4433d26d6389e88bfac/Modeling-of-pedestrian-movement-around-90-and-180-degree-bends.pdf (accessed January 15, 2023).

Sussman, A., Hollander, J.B., 2021. Cognitive architecture: Designing for how we respond to the built environment. Routledge.

Thompson, P.A., Marchant, E.W., 1995. Testing and application of the computer model 'SIMULEX'. Fire Saf. J. Volume 24, 149–166. https://doi.org/10.1016/0379-7112(95)00020-T, 1 1.

Thunderhead Engineering, 2022. *Pathfinder Technical Reference Manual.* [Online] Available at: https://www2.thunderheadeng.com/files/com/pathfinder/tech_ref.pdf (accessed April 17, 2023).

Torrens, P. M., 2009. Cellular Automata. In: *International Encyclopedia of Human Geography* Elsevier, 2009. https://doi.org/10.1016/B978-008044910-4.00411-9.

UN Population Division, 2007. *World urbanization prospects: the 2007 revision.* http://Esa.Un.Org/Unup. (2007).

Varas, A., Cornejo, M.D., Mainemer, D., Toledo, B., Rogan, J., Muñoz, V., Valdivia, J.A., 2007. Cellular automaton model for evacuation process with obstacles. Physica A: Statistical Mechanics and its Applications 382, 631–642. https://doi.org/10.1016/J.PHYSA.2007.04.006, 15 8.

Zanlungo, F., Feliciani, C., Yücel, Z., Jia, X., Nishinari, K., Kanda, T., 2023a. A pure number to assess "congestion" in pedestrian crowds. Transportation Research Part C: Emerging Technologies 148, 104041. https://doi.org/10.1016/J.TRC.2023.104041.

Zanlungo, F., Feliciani, C., Yücel, Z., Nishinari, K., Kanda, T., 2023b. Macroscopic and microscopic dynamics of a pedestrian cross-flow: Part II, modelling. Saf. Sci. 158, 105969.